Midcell localization of PBP4 of *Escherichia coli* is essential for the timing of divisome assembly

Jolanda Verheul[1#], Adam Lodge[2,7#], Hamish C.L. Yau[2,8#], Xiaolong Liu[1,9#], Alexandra S. Solovyova[3], Athanasios Typas[4,5] Manuel Banzhaf[6*], Waldemar Vollmer[2**], and Tanneke den Blaauwen[1***]

[1]Bacterial Cell Biology, Swammerdam Institute for Life Sciences, Faculty of Science, University of Amsterdam; Science Park 904, 1098 XH Amsterdam, The Netherlands.
[2]Centre for Bacterial Cell Biology, Biosciences Institute, Newcastle University, Newcastle upon Tyne, NE2 4AX, United Kingdom.
[3]NUPPA, Leech Building, Framlington Place, Newcastle upon Tyne NE2 4HH, UK
[4]European Molecular Biology Laboratory, Genome Biology Unit, Heidelberg, Germany
[5]European Molecular Biology Laboratory, Structural & Computational Unit, Heidelberg, Germany
[6]Institute of Microbiology & Infection and School of Biosciences, University of Birmingham, Edgbaston, Birmingham, UK. B15 2TT
[7]Present address: Iksuda Therapeutics, The Biosphere, Draymans Way, Newcastle Helix, Newcastle upon Tyne, NE4 5BX, UK
[8]Pressent address: Procter & Gamble, Newcastle Innovation Centre, Whitley Road, Newcastle-Upon Tyne, NE12 9TS, UK.
[9]Department of Biochemistry, University of Oxford, OX1 3QU, Oxford, United Kingdom.

[#]contributed equally.
*Corresponding author. Tel: +44 121 4145586; Email: m.banzhaf@bham.ac.uk
**Corresponding author. Tel: +44 191 208 3216; Email: w.vollmer@ncl.ac.uk
***Corresponding author. Tel: +31 20 525 3852; Email: t.denblaauwen@uva.nl

Running title: PBP4 is essential for divisome assembly timing

ABSTRACT (203 words)

Insertion of new material into the *Escherichia coli* peptidoglycan (PG) sacculus between the cytoplasmic membrane and the outer membrane requires a well-organized balance between synthetic and hydrolytic activities to maintain cell shape and avoid lysis. The hydrolytic enzymes outnumber the enzymes that insert new PG by far and very little is known about their specific function. Here we show that the DD-carboxy/endopeptidase PBP4 localizes in a PBP1A/LpoA and FtsEX dependent fashion at midcell during septal PG synthesis. Midcell localization of PBP4 requires its non-catalytic domain 3 of unknown function, but not the activity of PBP4 or FtsE. Domain 3 is also needed for the interaction of PBP4 with NlpI, but not for its interactions with PBP1A or LpoA. Microscale thermophoresis with isolated proteins

shows that domain 3 is needed for the interaction with NlpI, but not PBP1A or LpoA. *In vivo* crosslinking experiments confirm the interaction of PBP4 with PBP1A and LpoA. We propose that PBP4 functions together with the amidases AmiA and B to create denuded glycan strands to attract the initiator of septal PG synthesis, FtsN. Consistent with this model, we found that the arrival of FtsN and other cell division proteins at midcell was significantly delayed in cells lacking PBP4.

IMPORTANCE (140 words)

Peptidoglycan biosynthesis is a major target for antibacterials. The covalently closed peptidoglycan mesh, called sacculus, protects the bacterium from lysis due to its turgor. Sacculus growth is facilitated by the balanced activities of synthases and hydrolases, and disturbing this balance leads to cell lysis and bacterial death. Because of the large number and possible redundant functions of peptidoglycan hydrolases, it has been difficult to decipher their individual functions. In this paper we show that the DD-endopeptidase PBP4 localizes at midcell during septal peptidoglycan synthesis in *Escherichia coli* and is important for the timing of the assembly of the division machinery. This shows that inhibition of certain hydrolases could weaken the cells and might enhance antibiotic action.

KEYWORDS:, bacterial cell division, endopeptidase, immunolabeling, LpoA, NlpI, PBP1A, PBP4, peptidoglycan, preseptal, protein interactions

INTRODUCTION

The peptidoglycan (PG) layer is sandwiched between the cytoplasmic membrane (CM) and the outer membrane (OM) of the Gram-negative bacterium *Escherichia coli* forming a

66 covalently closed network of glycan strands that are interconnected by short peptides (1).
67 The PG layer maintains the shape of the bacterium by stabilizing the cell against its high
68 internal osmotic pressure. To proliferate, the rod-shaped bacterium grows in length and then
69 divides by binary fission into two equally sized daughter cells. The balanced activities of PG
70 synthases and hydrolases ensures a safe extension of the PG layer without defects that would
71 cause cell lysis (2). Beta-lactam antibiotics disturb this balance by inactivating the
72 transpeptidase (TPase) activity of the penicillin binding proteins (PBP)s causing lysis of
73 growing cells. We currently know more than twenty PG hydrolases that can cleave either in
74 the glycan chains or peptides within the PG layer, but how their activities are regulated is
75 poorly understood. This is particularly true for the PG endopeptidases (2). Recently, the OM
76 bound lipoprotein NlpI was shown to interact with similar affinity with several
77 endopeptidases, suggesting that NlpI acts as an interaction hub for endopeptidases to
78 regulate their activities by competing protein-protein interactions. (3).

79 The basic precursor (lipid II) for PG synthesis is the β-(1,4) linked disaccharide *N*-
80 acetylglucosamine-*N*-acetylmuramic acid (Glc*N*Ac-Mur*N*Ac) with an undecaprenol-
81 pyrophosphate linked to C1 of Mur*N*Ac and a stem peptide with the sequence L-alanine-D-
82 *iso*-glutamate-diaminopimelic acid (Dap)-D-alanine-D-alanine coupled to the C3 of Mur*N*Ac.
83 Lipid II is used by glycosyltransferases (GTases), which polymerize the glycan chains, and
84 TPase, which crosslink the stem peptides. The main PG synthases in *E. coli* are the class A PBPs
85 (PBP1A and PBP1B) with GTase and TPase activities (4-7), the integral membrane proteins
86 RodA and FtsW that have GTase activity (8-10) and monofunctional Class B PBPs (PBP2 and
87 PBP3) that have TPase activity (11-13).

88 The hydrolases are present in greater redundancy than the synthases (2, 14). The
89 carboxypeptidases (CPase) PBP5, 6A and 6B remove the terminal D-Ala of the nascent

90 pentapeptide (15-Popham:2003uc; 19). The endopeptidases (EPases) PBP4, PBP7, MepA,
91 MepM, MepH, and MepS cleave the crosslinks in the PG (19-21). The amidases AmiA-D
92 hydrolyze the bond between Mur*N*Ac and L-alanine at position 1 of the stem peptide (22-25).
93 Finally, the lytic transglycosylases Slt70 and MltA-G cleave the glycan strands to release 1,6-
94 anhydroMur*N*Ac containing turnover products (26-28). The large number of hydrolases
95 reflects the adaptability to various environmental conditions but begs the question of how
96 their potentially dangerous activities are controlled to avoid cell lysis.

97 Binary fission in *E. coli* is initiated by the assembly of the Z-ring at midcell, which
98 consist of a network of dynamic FtsZ filaments that are anchored to the cytoplasmic
99 membrane by FtsA and ZipA (29). The Z-ring also recruits the PG synthases PBP1A and PBP1B
100 to midcell (30). A number of Z-associated proteins play a role in the organization and
101 dynamics of the ring (31-35). Of these, the integral membrane protein FtsX interacts with FtsA
102 (36) and its cytoplasmic ATPase partner protein FtsE interacts with FtsZ (37). Both localize
103 early to midcell, together with the Z-ring (22). As a complex FtsEX recruits EnvC, which
104 activates AmiA and AmiB that are needed for septum cleavage (24, 38). FtsE versions without
105 ATPase activity still localize at midcell and recruit as FtsEX-EnvC complex but the latter is not
106 able to activate the amidases (39). Presumably an ATPase dependent conformational change
107 in FtsEX induces a conformational change in EnvC, which is then able to relieve an
108 autoinhibitory alpha-helix from the active site of AmiA and AmiB, activating them (40). The
109 third amidase AmiC is activated by the OM-anchored lipoprotein NlpD (22, 41). The
110 recruitment of the other cell division proteins occurs with a time delay of about 20% of the
111 cell division cycle, depending on the growth condition (42-45). FtsK, FtsBLQ, FtsW, PBP3 and
112 FtsN localize in an interdependent fashion. FtsBLQ inhibit the PG synthase activity of PBP3,

113 FtsW and PBP1B until they are outcompeted by the accumulation of FtsN that relieves this
114 inhibition and initiates septum synthesis (46-50).

115 While investigating the specific function of various PG hydrolases, we found that PBP4
116 localizes specifically at midcell as part of the division machinery. PBP4 is a periplasmic
117 endopeptidase (51) with a C-terminal amphipathic alpha-helix that associates with
118 membranes (52). Deletion of *dacB*, which encodes PBP4, does not have morphological
119 consequences but causes a decrease in the percentage of PG crosslinks and of PG-attached
120 lipoprotein (53) and an increased sensitivity to bile salts (54). Overproduction of PBP4 is toxic
121 (55) presumably because the enhanced cleavage of peptide cross-links weakens the PG mesh
122 and eventually causes lysis. PBP4 has three domains that are assembled in an unusual way
123 (56) (Fig. 1A). A non-catalytical domain of unknown function (domain 2) is inserted into the
124 transpeptidase domain 1, and a third domain (domain 3) is inserted into domain 2. Domain 3
125 is positioned above the active side with its catalytic serine 62, which resides in domain 1, and
126 might be involved in substrate binding or regulation (56, 57) (Fig. 1A). Side directed
127 mutagenesis suggested that residues from domain 1 (R361) and 2 (D155) are important for
128 the endopeptidase activity (58).

129 Here we determined the localization of PBP4 and different variants during the cell
130 cycle of *E. coli.* The timing of localization at midcell and interactions of PBP4 support a role in
131 remodeling of PG synthesized by the divisome.

132

133 **RESULTS**
134
135 **PBP4 localizes to the lateral wall and at midcell.** To determine the localization of PBP4 in *E.*
136 *coli* cells as a function of the bacterial cell cycle, we generated an antiserum against PBP4 and
137 removed unspecific antibodies by adsorption to cells of a *dacB* mutant strain that lacks PBP4.

138 The purified antibodies were specific for PBP4 (Fig. S1) and used to immunolabel the wild-
139 type strain MC4100 grown in rich (TY) medium at 37°C. PBP4 localized strongly at midcell and
140 to a lesser extend in the lateral wall in wild-type cells (Fig. 1B).

141 **PBP4 localizes between the peptidoglycan layer and the outer membrane**. Although
142 it was reported that PBP4 has a stretch of weakly amphipathic amino acids at its C-terminus
143 (52), it was not known whether PBP4 is freely diffusing in the periplasm or associates with the
144 membrane or other proteins. It has been previously observed that chemically fixing freely
145 diffusing periplasmic proteins can shock them into the cell poles (11, 59). The fact that we did
146 not observe any polar localization of PBP4 after fixation (Fig. 1B and S1), suggests that it is
147 either associated with the membrane or other proteins. Next, we investigated whether PBP4
148 was accessible to anti-PBP4 in cells with an intact PG layer. For this, wild-type cells were grown
149 in TY at 37°C and immunolabeled without Triton X-100 permeabilization of the OM or without
150 increasing the pore size of the PG mesh with lysozyme. PBP4 was not accessible without
151 permeabilization of the OM, but was fully accessible in cells with an intact PG (Fig. 1C). In
152 contrast, proteins like FtsN and PBP3 were not accessible without degradation of the PG layer
153 by lysozyme (Fig. 1C). This suggests that PBP4 resides between the OM and the PG layer.

154 **Activity of PBP4 is not needed for midcell localization.** Substrate binding can be a key
155 determinant in the localization of proteins (16, 60, 61). To test whether PBP4 substrate
156 binding is needed to localize at division sites we expressed the active site mutant PBP4S62G
157 or A (57) that fails to bind β-lactams and therefore is not able to hydrolyze the PG stem
158 peptide (Fig. S2 and S3). A plasmid encoding the mutant protein was constitutively expressed
159 in a Δ*dacB* background by the leakage of a weakened p*Trc99*A promoter. Interestingly, the
160 wild-type and active site mutant when expressed from plasmid were both able to localize at
161 midcell (Fig. 2). This indicates that although PBP4(S62G/A) cannot hydrolyze its substrate or

162 bind β-lactams covalently (Fig. S2C Fig. S3), it is either still able to interact with its substrate
163 or it localizes through protein interactions.

164 Since PBP4(S62G/A) likely still interacts with its substrate, we mutagenized the gene
165 to replace two residues (D155 and R361; (58)) involved in the binding of the DAP residue in
166 the stem peptide by alanine. The genes encoding PBP4(D155A) or PBP4(R361A) were
167 expressed by promoter leakage from plasmid in a Δ*dacB* background, and both PBP4 versions
168 localized at midcell (Fig. 2). An immunoblot analysis showed that all mutants were expressed
169 to similar levels and that PBP4(R361A) and PBP4(D155A) were able to bind the fluorescent β-
170 lactam Bocilin-FL (Fig. S2). Therefore, all three active site protein variants are potentially able
171 to still interact with substrate as an inactive protein.

172 A PBP4 version lacking domain 3 (PBP4ΔD3) was still able to bind β-lactams (Fig. S2B
173 and S3) but did not have DD-carboxypeptidase or DD-endopeptidase activity (Fig. S3).
174 Analytical ultracentrifugation (Fig. S4A) and circular dichroism analysis (Fig. S4B) of isolated
175 PBP4ΔD3, showed that the removal of domain 3 did not affect the structure, the dimerization
176 of the rest of the protein or its interaction with PG sacculi (Fig. S4C), which suggests a folded
177 active site domain. However, the inactive but substrate binding PBP4ΔD3 was not localizing
178 at midcell (Fig. 2). Hence, we conclude that PBP4 localization could be largely driven by
179 protein interactions and to a lesser extent by substrate interaction but is independent from
180 its own activity.

181 **PBP4 localizes weakly at inactive divisomes.** To further dissect whether the
182 localization of PBP4 at the division site is dependent on the availability of its substrate or on
183 the physical presence of other proteins at the division site, cell division was inhibited through
184 inactivation of PBP3 by its specific inhibitor aztreonam (62). Aztreonam treatment for about
185 two mass doublings stalls the division machinery at midcell resulting in filamentous growth.

186 In the longer filaments new division machineries are formed and localize at future division
187 sites (5). In these filaments PBP4 localized weakly at all possible division sites (Fig. S5),
188 indicating that the activity of PBP3 was not required for the localization of at least some PBP4
189 molecules. While PBP3 is inhibited, preseptal PG synthesis (63) still occurs at the potential
190 division sites in the filamenting cells (30, 64, 65). The localization of PBP4 could therefore be
191 associated with the presence of PBP1A or PBP1B, which were previously shown to be
192 recruited to preseptal PG synthesis sites by early cell division proteins (Pazos:2018fj).

193 **PBP1A/LpoA assist in midcell localization of PBP4.** PBP4 was recently reported to
194 interact with PBP1A, LpoA and the EPase adaptor protein NlpI (3). To investigate whether
195 PBP1A and/or LpoA proteins were needed for midcell localization of PBP4, strains deleted for
196 *mrcA* (PBP1A), *lpoA*, *mrcB* (PBP1B) or *lpoB* were grown in rich medium at 37°C and
197 immunolabeled with anti-PBP4. The amount of PBP4 that localized at midcell was identical
198 for the parental wild-type strain BW25113, Δ*mrcB* and Δ*lpoB,* but reduced in the Δ*mrcA* and
199 Δ*lpoA* strains, whereas the PBP4 concentration was similar for all strains (FIG. 3). This could
200 indicate that PBP1A/LpoA assist in the initial localization of PBP4 at midcell.

201 **NlpI seems not to be involved in midcell localization of PBP4**. We next tested if the
202 interaction with NlpI affected the localization of PBP4. In the Δ*nlpI* cells the amount of PBP4
203 at midcell per μm average cell circumference was reduced with 42 ± 6.7% (n=3) compared to
204 wild type and the protein localized later at midcell than in the wild-type cells (Fig. S6). The
205 PBP4 concentration in the Δ*nlpI* strain was also lower than in the wild-type cells (64.8 ± 17.6%,
206 n= 3). This could indicate that the cells down-regulate PBP4 expression or that PBP4 becomes
207 unstable in the Δ*nlpI* strain. Interestingly, labeling of PBP4 in a Δ*nlpI* strain also did not require
208 lysozyme (Fig. S6), suggesting that one or more additional interactions maintains PBP4
209 localized outside the PG layer.

210 **PBP4 domain 3 facilitates interaction with NlpI but not PBP1A/LpoA**. Microscale
211 thermophoresis (MST) in which one protein is labelled with a fluorophore and titrated with
212 an unlabeled partner protein was used to analyze the interactions between PBP4 and its
213 known interaction partners further. The difference in thermophoresis of the complex versus
214 the unbound fluorescently labeled proteins is then used to calculate the affinity of the binding
215 partners. Different versions of PBP4 and its interaction partners were purified and assayed
216 for direct protein-protein interactions. Wild-type PBP4 interacted with PBP1A, LpoA and NlpI
217 (3). PBP4 lacking domain 3 (PBP4ΔD3), which did not localize at midcell (Fig. 2), interacted
218 with PBP1A and LpoA but not with NlpI (Fig. 4). These results suggest that domain 3 of PBP4
219 facilitates the interaction with NlpI, but not PBP1A.

220 **NlpI and PBP1A/LpoA have different binding sites in PBP4.** PBP4 can form a multi-
221 enzyme complex with NlpI and PBP1A/LpoA (3). PBP1A interacted with PBP4 and could be
222 cross-linked to PBP4 in cells (Fig. 4C). We found that full length LpoA interacted with both
223 PBP4 and PBP4ΔD3, with apparent K_D values of 315 ± 38 nM and 153 ± 31 nM, respectively
224 (Fig. 4A; Fig. S7). This suggests that domains 1 or 2 of PBP4 are sufficient for the interaction
225 with LpoA. MST assays of PBP4 or PBP4ΔD3 with LpoA's C-terminal (residues N257-S678;
226 $LpoA^C$) or N-terminal (LpoA residues G28-T256; $LpoA^N$) domains also yielded positive binding
227 curves (Fig. 4A; Fig. S7) (66-68). We found that $LpoA^C$ and the full length LpoA version had
228 comparable affinities for both PBP4 versions, suggesting that the C-terminal domain of LpoA
229 is sufficient for interaction with PBP4 (Fig. 4A). Interestingly, the removal of domain 3 from
230 PBP4 resulted in an increased affinity of $LpoA^N$ for PBP4 (app. K_D decreased by ~50 fold) (Fig.
231 4A Fig. S7). Hence, the interaction between the N-terminal domain of LpoA and PBP4 possibly
232 occurs via a different mechanism dependent on a conformational rearrangement of domain
233 3 of PBP4. This suggests that the two domains of LpoA, which likely serve different primary

234 functions, are both sufficient for an interaction with PBP4, albeit with varying affinities. In
235 conclusion PBP4 robustly interacts with PBP1A/LpoA independent of its domain 3.

236 **LpoA has a small effect on PBP4 activity**. We found previously that NlpI does not
237 affect PBP4 activity (3) but considered it possible that PBP4 interaction with PBP1A/LpoA may
238 affect its activity. We first verified that NlpI or PBP4 did not affect the activity of PBP1A in the
239 presence or absence of LpoA using an *in vitro* glycosyltransferase assay (Fig. 5). We next
240 tested if PBP1A or LpoA affected the activity of PBP4 using *in vitro* PG degradation assays.
241 LpoA decreased the activity of PBP4 by about 30% in a continuous DD-CPase assay with
242 soluble substrate and an endpoint PG digestion assay (Fig 5B and C). To assess whether LpoA
243 also affects PBP4 activity *in vivo*, a Δ*dacB*Δ*lpoA* strain and Δ*dacB* strain were transformed
244 with the plasmids expressing PBP4 or the active site mutant PBP4(S62G) and the toxicity of
245 their expression was compared. Although the double mutant was less fit than the single
246 mutant, it was equally sensitive to the overexpression of PBP4 (Fig. 5D), leaving no indication
247 that LpoA also inhibits the activity of PBP4 *in vivo*.

248 **PBP4 localizes as early and late divisome protein.** Since PBP4 localizes at midcell it
249 could be part of or associated with the divisome. The division machinery is assembled in two
250 in time separated steps (42, 69). First, FtsZ and its membrane bound partners ZipA and FtsA
251 in conjunction with other Z-ring associated proteins form the proto-ring that localizes at
252 midcell (70). Second, after approximately 20% of the cell division cycle the remaining proteins
253 assemble subsequently at the division site. To obtain more details on PBP4 localization in
254 relation to other cell division proteins, MC4100 cells were grown to steady state in minimal
255 glucose medium at 28°C. The cells were immunolabeled with antibodies again PBP4 and
256 against FtsZ, PBP3, and FtsN that localize early, late and last, respectively. PBP4 localized
257 strongly at midcell and hardly in the lateral cell wall (Fig. 6). To determine whether PBP4

258 belongs to the early or late divisome localizing proteins, we analyzed the timing of its midcell
259 localization. To this end, we plotted the extra fluorescence (FCPlus) present at midcell in
260 comparison to the amount of fluorescence in the rest of the cell (Fig. 6B and C). PBP4 localized
261 together with the late localizing proteins like PBP3 and FtsN, but close inspection of its
262 localization timing shows that it arrives in a small amount at 30% of the cell cycle in between
263 FtsZ and PBP3 (Fig. 6C). After 40% it shows about the same timing as PBP3. This could indicate
264 that PBP4 localizes relatively early and dependent on the amount of substrate produced.

265 **Midcell localization of PBP4 depends on FtsE**. To investigate if PBP4 localization is
266 dependent on division associated proteins we localized PBP4 in different temperature
267 sensitive strains. Strains were grown in minimal glucose medium at 28°C to an OD_{450} of 0.2,
268 diluted 1:4 in prewarmed medium of 28°C or 42°C and grown for two mass doublings before
269 PBP4 immunolabelling. PBP4 localized in filamentous cells with thermo-labile FtsQ, FtsW or
270 PBP3 indicating that these proteins are not involved in the recruitment of PBP4 (Fig. 7). In
271 filamentous *ftsA*(ts) cells PBP4 localized mostly at one or two division sites, although these
272 cells had 4 to 8 potential division sites. We suspected that the level of remaining FtsA was
273 sufficient to assemble only one or two Z-rings at the non-permissive temperature. Labeling of
274 the filamentous *ftsA*(ts) cells with antibodies against FtsZ showed indeed a similar localization
275 frequency of FtsZ and PBP4 (Fig. 7). This shows that PBP4 needs FtsZ and FtsA for localization
276 in agreement with our previous finding of localizing after FtsZ (Fig 6 C).

277 PBP4 localized only weakly at division sites in the filamentous *ftsE*(ts) cells (Fig. 7). This
278 suggests that a functional FtsE is important for PBP4 localization. The FtsEX/EnvC complex
279 assists in the assembly of the divisome (71, 72) and is essential for amidase function to cleave
280 PG for cell separation (39). To investigate a possible link between PBP4 and this complex we
281 further dissected PBP4's localization pattern. PBP4 localized at division sites in a Δ*envC* strain,

282 indicating that EnvC is not needed for PBP4 localization. However, PBP4 failed to localize in a
283 Δ*ftsEX* strain (Fig. 8). To verify whether FtsE and FtsX were required for PBP4 localization we
284 constructed a Δ*ftsE* strain. The *ftsE* and *fts*X genes reside in an operon and the expression of
285 *fts*X requires the *fts*E gene (73). We therefore constructed a Δ*ftsE* strain with a weakened
286 p*Trc*99A promoter placed upstream of *fts*X to ensure sufficient expression of FtsX. The
287 resulting strain, XL36 grew with a mild filamentous phenotype in rich medium that could be
288 complemented by the expression of FtsE(wt) (Fig S9). PBP4 localized weakly at septal
289 positions in the Δ*fts*E strain XL36 but localized normally when FtsE was expressed to
290 complement this strain (Fig 8B). This suggests that FtsE and FtsX enhance the septal
291 localization of PBP4. Interestingly, PBP4 localized at division sites in a strain lacking the three
292 amidases AmiA, AmiB and AmiC (Fig. S10) and in a strain lacking essential components of the
293 Tol-Pal system, which is involved in the coordination of OM constriction and PG invagination
294 during cell division (Fig. S10).

295 **Activity of FtsE is not required for midcell localization of PBP4.** The failure of PBP4 to
296 localize in the FtsE(ts) variant could be due to unstable or inactive FtsE localizing at the
297 division site. Sequencing of the gene revealed a C to T base pair change that is predicted to
298 cause Pro135 to be replaced by Ser in the FtsE protein. To determine the role of this mutation,
299 the sequence of the ABC transporter Mi0796 of *Methanococcus jannashii* for which a crystal
300 structure is available (PDB code 1L2T (74)) was aligned with the amino acid sequence of *E. coli*
301 FtsE using Clustal W (75). Pro135 is part of a loop preceding a small alpha-helix adjacent to
302 the walker B motif that is needed for ATP binding and hydrolysis. We therefore assumed that
303 the mutation affected the ATP binding or hydrolysis but not the cellular localization of the
304 protein. To validate this hypothesis, a wild-type parental strain LMC500 and the Δ*ftsE* strain
305 XL36 were transformed with the plasmids expressing FtsE(wt) or the thermosensitive FtsE(ts)

306 fused to the fluorescent protein (FP) mNeonGreen (mNG), and were grown at both permissive
307 and non-permissive temperatures. mNG-FtsE localized at midcell in wild-type and Δ*ftsE*
308 strains and was able to restore wild-type morphology apart from few cells that filamented.
309 FP-FtsE(ts) was not able to localize in the Δ*ftsE* XL36 at non-permissive temperature. Even at
310 the permissive temperature localization was not restored implying that localization is further
311 weakened by the FP and the absence of an endogenous FtsE. Localization of PBP4 was
312 restored in the XL36 (Δ*ftsE*) expressing mNG-FtsE(wt) background (Fig. S9). As it is unclear
313 whether FtsE(wt) lacks stability or activity or both, we expressed three inactive mutants that
314 had been shown to localize to midcell (73). We tested PBP4 localization in those strains to
315 discriminate whether or not FtsE activity is needed for its localization. The K41Q and D162A
316 versions of FtsE cannot bind ATP and FtsE(E163A) binds ATP but cannot hydrolyze it. In
317 contrast to what was shown previously, we found that mNG-FtsE versions unable to bind ATP
318 did not localize to midcell. FtsE(E163A) is able to bind ATP and localized at division sites in
319 filamentous Δ*ftsE* cells. PBP4 followed the localization pattern of FtsE versions suggesting that
320 ATP hydrolysis by FtsE is not a requirement for localization of PBP4. Because the mNG seemed
321 to affect the localization of FtsE somewhat, the experiments were repeated with published
322 untagged FtsE versions (73). PBP4 localized in all four FtsE active site mutants (Fig. 8B)
323 showing that the activity of FtsE is indeed not required for the localization of PBP4.

324 **PBP4 affects the timing of the divisome assembly.** To measure the timing of divisome
325 in various strain backgrounds, we grew Δ*dacB* cells carrying either an empty plasmid or
326 plasmids constitutively expressing PBP4 or PBP4 versions to steady state in minimal glucose
327 medium at 28°C. Cells were fixed, divided into three aliquots and were labeled with anti FtsZ,
328 anti PBP4 or anti FtsN. We determined the timing of the arrival of these proteins at midcell
329 by analyzing fluorescence signals of several thousands of cells (76). In the parental strain FtsZ

330 and FtsN started to localize at midcell at about 29% and 50% of the cell cycle age, respectively.
331 Similarly, in the Δ*dacB* strain expressing wild-type PBP4 from plasmid FtsZ and FtsN started
332 to localize at midcell at about 20% and 49% of the cell division cycle age, respectively (Fig. 9D).
333 Strikingly, all three proteins localized simultaneously and very late at 45% of the cell division
334 cycle time in the Δ*dacB* strain (Fig. 9D). Expression of inactive PBP4 versions affected the
335 timing of the divisome assembly as well. Especially Δ*dacB* cells expressing PBP4(D155A) from
336 plasmid, which was slightly filamentous (Fig. 9B), assembled the divisome very early and
337 showed a longer cell division period. These results show that PBP4 profoundly affects the
338 timing of divisome assembly.
339
340 **DISCUSSION**
341
342 *Escherichia coli* contains a large number of seemingly redundant PG hydrolases, which
343 possibly fine tune peptidoglycan biogenesis and remodelling in response to environmental
344 parameters. Apart from their enzymatic activities, little is known about the actual function of
345 most PG hydrolases. Here we report that the DD-endopeptidase PBP4 localizes at midcell
346 during septal peptidoglycan synthesis in *E. coli* and is important for the timing of the assembly
347 of the division machinery.
348 **PBP4 localises at midcell during cell division in an FtsEX dependent manner.** PBP4
349 localizes predominantly at midcell during cell division in an FtsEX dependent manner. Inactive
350 PBP4 variants were able to localize at midcell indicating that substrate hydrolysis is not a
351 requirement for localization. However, a version of PBP4 lacking the non-catalytic domain 3
352 (PBP4ΔD3), which is required for activity but not β-lactam binding, did not localize to mid-cell.
353 From these results we infer that PBP4 localizes to midcell either by recognizing its substrate

354 (without the need to hydrolyse it) and/or by protein-protein interactions. Our data also
355 suggest that the bulk of PBP4 localizes late at the division site. Nevertheless, some PBP4
356 molecules appear to arrive early and may associate to preseptal PG synthesis, which is
357 consistent with the observation that PBP4 is required for the timing of divisome assembly and
358 cell division (Fig 1).

359 **PBP4 might be involved in preseptal PG synthesis.** PBP4 interacts with NlpI, PBP1A
360 and LpoA and these proteins are able to form a ternary complex ((3) and (Fig. 4). PBP4ΔD3
361 interacted with PBP1A and LpoA but not with NlpI, confiming differential PBP4 binding sites
362 of PBP1A, LpoA and NlpI. The interaction with PBP1A and/or LpoA may contribute to the
363 recruitment of PBP4 at midcell, as the amount of PBP4 at midcell was slightly reduced in
364 Δ*mrcA* and Δ*lpoA* strains. PBP1A and its partner LpoA are involved in preseptal PG synthesis
365 (30, 76). PBP4 weakly localizes at preseptal sites in cell filaments generated with aztreonam
366 that have lost septal synthesis but not preseptal synthesis activity. Possibility, some PBP4
367 enriches at preseptal PG synthesis sites together with PBP1A/LpoA, which localize through
368 the interaction of PBP1A with ZipA (30), and preseptal PG synthesis provide substrates for
369 PBP4. The interaction between NlpI and PBP4 could function to sequester PBP4 in the lateral
370 wall to prevent its interaction with potential substrate (Fig. 10).

371 **Why does the loss of PBP4 affects the timing of divisome assembly?** The absence of
372 PBP4 severely interferes with the timing of the divisome assembly. In most bacteria studied
373 thus far, the Z-ring with its associated early division proteins localizes first to prepare the
374 future cell division site, perhaps by generating the border between the side wall and the
375 future septum (30, 63, 65). After a time delay, the proteins that synthesize the bulk of the
376 septal PG arrive and septation starts (42-45). In the absence of PBP4, there is no time delay
377 between the early and late cell division proteins and a late arrival of FtsZ coincides with the

378 arrival of FtsN and the initiation of septal PG synthesis. This change of divisome assembly
379 could be caused by direct or indirect effects. PBP4 could be directly needed to open the PG
380 layer to allow insertion of new septal material or to remodel the nascent PG to allow new
381 insertions. Alternatively, the absence of PBP4 might enable NlpI to bind other EPases,
382 coordinating their activity for remodelling the PG layer during septation. However, the robust
383 localization of PBP4 at midcell suggests a direct function for PBP4 in PG remodelling. We
384 hypothesise that during elongation sufficient PBP4 molecules are retained by NlpI in the
385 lateral wall above the PG layer to avoid promiscuous PBP4 activity (Fig. 10). This is consistent
386 with the observations that the absence of NlpI resulted in a reduced amount of PBP4 present
387 in the cells (Fig. S6 and (3)). NlpI is not enhanced at midcell (3) and therefore we do not
388 anticipate a role for NlpI in the retention of PBP4 at midcell. PBP4 might be initially recruited
389 to midcell through interactions with PBP1A and LpoA, and possibly the FtsEX-EnvC complex,
390 likely directing PBP4's activity already to preseptal sites (Fig. 10). Once septal peptidoglycan
391 synthesis starts by the mature divisome, more substrate should become available for PBP4
392 facilitating its accumulation at midcell, which we observed in the immunolocalization
393 experiments. Hence, PBP4 could initially remove crosslinks to help AmiA and AmiB to
394 generate denuded glycan strands. These would facilitate the accumulation of FtsN, which is
395 required to initiate septal PG synthesis. Alternatively, PBP4 could simply remove old glycan
396 strands during preseptal PG synthesis. Because of its impact on the timing of the divisome
397 assembly, the first option seems to be more likely. Whether the function of PBP4 remains the
398 same during septation will need further investigation.
399

400 **MATERIALS AND METHODS**
401

402 **Culturing conditions.** *E. coli* K12 cells were grown to steady state (76) in glucose minimal
403 medium containing 6.33 g of $K_2HPO_4.3H_2O$, 2.95 g of KH_2PO_4, 1.05 g of $(NH_4)_2$, 0.10 g of
404 $MgSO_4.7\ H_2O$, 0.28 mg of $FeSO_4.7\ H_2O$, 7.1 mg of $Ca(NO_3)_2.4\ H_2O$, 4 mg of thiamine and 4 g of
405 glucose per L. For strain MC4100 and its derivatives 50 µg lysine (Gb1) and for BW25114 and
406 MG1655 derivatives 2 µg uracil, 20 µg thymidine, 50 µg arginine and glutamine (Gb4) per liter
407 pH 7.0 at 28°C or 37°C were added. Absorbance was measured at or 450 nm with a 300-T-1
408 spectrophotometer (Gilford Instrument Laboratories Inc.). Alternatively, cells were grown in
409 TY (5g yeast extract, 10 g bacto trypton and 85 mM NaCl, pH 7.0), or LB, which is TY with 170
410 mM NaCl and absorbance was measured at 600 nm.

411 **Strain construction.** Strain XL35, the FtsE partial deletion strain, was constructed as
412 follows: Primers priXL221 and priXL222 was used to amplify the upstream homologous
413 sequences (*UHS*) from the *ftsE* start codon, and primers priXL223 and priXL224 were used to
414 amplify the downstream homologous sequence after the FtsE 151th amino acid (the potential
415 promoter of *ftsX*), from the MC4100 genome. Primers priXL51 and priXL54 were used to
416 amplify the kanamycin resistance cassette from plasmid pKD4 (77). The amplified overlap PCR
417 product (*UHS-FRT-KAN-FRT-DHS*) with primers priXL221 and priXL224 was used to construct
418 the recombinant strain XL34 in which the first 150 amino acids encoding sequencing of *ftsE*
419 was deleted (77). Subsequently, the kanamycin selection cassette was removed with plasmid
420 pCP20 (77) yielding XL35.

421 Strain XL36, the *ftsE* clean deletion strain, was constructed similarly as XL35. Primers
422 priXL221 and priXL222 were used to amplify the upstream homologous sequences from the
423 *ftsE* start codon, and primers priXL225 and priXL226 were used to amplify the downstream
424 homologous sequences after the *ftsE* stop codon, from the MC4100 genome. In order to
425 restore the FtsX expression, a *pTrc99Adown* promoter (78) was amplified from plasmid

426 pSAV057 (79) with primers priXL77 and priXL227 and a chloramphenicol selection cassette
427 was amplified from plasmid pKD3 with primers priXL52 and priXL54. The amplified overlap
428 PCR product (*UHS-FRT-CAM-FRT-DHS*) with primers priXL221 and priXL226 was used to
429 construct the recombinant strain XL33 in which the entire *ftsE* coding sequence was deleted
430 and FtsX was expressed from the chromosomally encoded p*Trc99Adown* promoter.
431 Subsequently, the kanamycin selection cassette was removed with plasmid pCP20 yielding
432 XL36 (Table 1).

433 **Plasmid construction**. The *ftsE* 1181(ts) mutation was amplified from the
434 chromosome of LMC515 (80) using the forward primer priXL187 and the reverse primer
435 priXL188, and sequenced to characterize the mutation. The mutated and the wild-type *ftsE*
436 genes were cloned into pSAV057, p15A origin and Cam^R (79) to produce the plasmids pXL135
437 and pXL136, respectively. *FtsE* was expressed under the control of the p*Tcr*99A down
438 promoter. QuickChange site directed mutagenesis (Agilent technologies, Santa Clara, CA) and
439 Gibson assembly (81) approaches were applied afterwards to construct the inactive *ftsE*
440 mutant plasmids pXL137, pXL138 and pXL139, using the primers listed in Table 2.

441 To construct the PBP4 expression plasmids, the wild-type *dacB* gene was firstly
442 amplified from the *E. coli MG1655* genome using primer priXL244 and priXL245, and
443 subsequently cloned into plasmid pSAV057 and pSAV057-$dsba^{ss}$-mCherry-PBP5 (pNM010 (18))
444 with *EcoRI* and *HindIII*, to generate the PBP4 plasmids without and with mCherry fusion.
445 Similarly, QuickChange site directed mutagenesis and Gibson assembly approaches were
446 applied afterwards to construct the inactive *dacB* mutant plasmids from these two wild-type
447 plasmids, using the primers listed in Table 2.

448 **Immunolabeling**. After reaching steady state for minimal glucose grown cells or the
449 desired OD for rich medium grown cells, the cells were fixed for 15 min by addition of a

450 mixture of formaldehyde (f. c. 2.8%) and glutaraldehyde (f. c. 0.04%) to the cultures in the
451 shaking water bath and immunolabeled as described (82) with Rabbit polyclonal antibodies
452 against PBP4 or NlpI (3) preabsorbed against *ΔdacB* or *ΔnlpI*, strains, respectively. As
453 secondary antibody, donkey anti-rabbit conjugated to Cy3 or to Alexa488 (Jackson
454 Immunochemistry, USA) diluted 1:300 in blocking buffer (0.5% (wt/vol) blocking reagents
455 (Boehringer, Mannheim, Germany) in PBS) was used, and the samples were incubated for 30
456 minutes at 37°C. For immunolocalization, cells were immobilized on 1% agarose in water slabs
457 coated object glasses as described (83) and photographed with an Orca Flash 4.0 (Hamamatsu,
458 Japan) CCD camera mounted on an Olympus BX-60 (Japan) fluorescence microscope through
459 a 100x/*N.A*. 1.35 oil objective. Images were taken using the program ImageJ with
460 MicroManager (https://www.micro-manager.org).

461 SIM images were obtained with a Nikon Ti Eclipse microscope (Japan) and captured
462 using a Hamamatsu Orca-Flash 4.0 LT camera. Phase contrast images were acquired with a
463 Plan APO 100x/1.45 Ph3 oil objective. SIM images were obtained with a SR APO TIRF
464 100x/1.49 oil objective, using 3D-SIM illumination with a 561nm laser, and were
465 reconstructed with Nikon-SIM software using the values 0.20-0.25-0.20 for the parameters
466 Illumination Modulation Contrast (IMC), High Resolution Noise suppression (HNS) and Out of
467 focus Blur Suppression (OBS), respectively.

468 **Image analysis.** Phase contrast and fluorescence images were combined into
469 hyperstacks using ImageJ (http://imagej.nih.gov/ij/) and these were linked to the project file
470 of Coli-Inspector running in combination with the plugin ObjectJ
471 (https://sils.fnwi.uva.nl/bcb/objectj/). The images were scaled to 15.28 pixel per μm. The
472 fluorescence background has been subtracted using the modal values from the fluorescence
473 images before analysis. Slight misalignment of fluorescence with respect to the cell contours

474 as found in phase contrast was corrected using Fast-Fourier techniques as described (76).
475 Data analysis was performed as described (76). In brief, midcell was defined as the central
476 part of the cell comprising 0.8 µm of the axis. From either cell part, midcell and remaining cell,
477 the volume, the integrated fluorescence, and thus the concentration of fluorophores was
478 calculated. The difference of the two concentrations is multiplied with the volume of midcell.
479 It yields FCPlus (surplus of fluorescence) at midcell. For age calculation, all cell lengths are
480 sorted in ascending order. Then the equation

481 age = ln(1 - 0.5 * rank / (nCells - 1)) / ln(0.5)

482 is used, where *rank* is a cell's index in the sorted array, *nCells* is the total number of cells, and
483 *age* is the cell's age expressed in the range 0 .. 1.

484 **Ni^{2+}-NTA pulldown assays**. Nickel-Nitrilotriacetic acid (Ni-NTA) coupled agarose beads
485 (Qiagen) were used in this assay to retain His-tagged proteins from protein mixtures. Similar
486 to affinity chromatography techniques, the His-tagged protein then becomes a secondary bait
487 protein to bind untagged interaction partners.

488 Ni-NTA beads (100µl) were pre-equilibrated with dH_2O and binding buffer (10 mM
489 HEPES/NaOH, 10 mM $MgCl_2$, 150 mM NaCl, 0.05% Triton X-100, pH 7.5) by centrifugation at
490 4000 × *g*, 4 min at 4°C, and then incubated with proteins of interest. Equimolar amounts (1-2
491 µM) of His_6-tagged and untagged proteins were incubated alone (control) and in combination,
492 for 10 min at 4°C in a 200 µl reaction volume, containing 10 mM binding buffer. An aliquot of
493 this mixture is taken as an 'applied' sample. The protein samples were then added to pre-
494 equilibrated Ni-NTA beads and incubated overnight on a spinning plate at 4°C with 1.3 ml of
495 binding buffer.

496 Beads were centrifuged at 4000 × *g*, 4 min, 4°C and washed a further 4-6 times with 1
497 ml of washing buffer (binding buffer with 30 mM Imidazole) before re-suspending in 250 µl

498 washing buffer and transferring beads to Proteus spin columns (Generon), centrifuging as
499 described above. Bound proteins were eluted by the addition of 50 µl of SDS-PAGE loading
500 buffer and boiling at 100°C for 5 min. Spin columns were centrifuged a final time at 1500 × *g*,
501 5 min, RT, to collect 'eluted' protein before separation by SDS-PAGE. Eluted samples were run
502 alongside applied samples for comparison.

503 **Microscale thermophoresis.** Microscale thermophoresis (MST) is an immobilisation-
504 free method which allows the detection of biomolecular interactions in solution. This
505 technique is based on the specific directed movement of a protein along a heat gradient
506 (thermophoresis), an observation first reported by Carl Ludwig in 1856 (84). The
507 thermophoresis of a protein changes upon ligand binding due to one or more changes to size,
508 charge and/or hydration shell. In MST, a localised heat gradient is initiated by an IR-laser
509 (wavelength 1470 nm). A protein of interest is fluorescently labelled and the change in its
510 thermophoretic mobility, in the presence of an unlabelled ligand, is measured and expressed
511 as a change in the normalised fluorescence (FNorm).

512 Proteins of interest (10-20 µM) were fluorescently labelled with an amine
513 reactive dye (NT-647- N-hydroxysuccinimide (NHS)), cysteine reactive dye (NT-647 maleimide)
514 or a histidine reactive dye (NT-647-Tris-NTA), according to manufacturer's instructions
515 (Nanotemper). Fluorescently labelled proteins were diluted to an appropriate concentration
516 and a fixed concentration was titrated against a two-fold serial dilution of unlabelled ligand,
517 across 16 samples, in MST running buffer (25 mM HEPES/NaOH, 150 mM NaCl, 0.05% Triton
518 X-100, pH 7.5).

519 MST measurements were carried out as described in (85), using standard or premium
520 capillaries on a Monolith NT.115^{TM} MST machine (Nanotemper). Binding curves and Kinetic
521 parameters were plotted and estimated using manufacturer provided software (NT Analysis

522 1.5.41 and MO. Affinity Analysis (x64)). Capillary scans were carried out prior to all
523 measurements to check for consistent fluorescence counts, confirming that any subsequent
524 change in fluorescence was due to ligand binding and not due to inaccurate pipetting or
525 adsorption and dilution effects.

526 **SDS-denaturation (SD) test.** In instances where capillary scans showed a ligand
527 concentration dependant change in raw fluorescence, we investigated whether this was a
528 property of the binding interaction by carrying out an SD-test.

529 Samples (10 uL) with the highest and lowest concentration of unlabelled ligand were
530 centrifuged 10 000 × *g,* 5 min, RT and mixed 1:1 volume ratio with SD-test buffer (40 mM DTT,
531 4% SDS). Mixtures were boiled at 100 °C for 10 min, to abolish ligand binding, before being
532 spun down and subjected to another capillary scan. If the fluorescence between samples that
533 contained the highest and lowest concentration of ligand, after SDS treatment, were now
534 back to ± 10% of each other, the initial observations were a property of ligand binding and a
535 binding curve was plotted from the raw fluorescence data. If the ligand concentration
536 dependent change in fluorescence was still observed, then this indicated that the
537 fluorescently labelled protein was aggregating and assay and buffer conditions were
538 optimised accordingly

539 ***In vivo* cross-linking / co-immunoprecipitation assays.** Method is described in, and
540 adapted from (86). An overnight culture of *E. coli* BW25113 cells and an appropriate mutant
541 strain was used to inoculate 150 ml of Lennox LB (Fisher Scientific) and was cultivated to an
542 OD_{578} of 0.5-0.6 at 37°C before harvesting by centrifugation (4500 × g, 4°C, 25 min). Cells were
543 resuspended in 6 ml of CL buffer 1 (50 mM NaH_2PO_4, 20% sucrose, pH 7.4). The amine reactive
544 cross-linker, DTSSP (3,3'-dithiobis (sulfosuccinimidylpropionate) (ThermoFisher), was freshly
545 dissolved (20 mg/ml in dH_2O) and added to the isolated cell suspension and incubated at 4°C

546 with agitation for 1 h. Cross-linked cells were then harvested by centrifugation (4500 × g, 4°C,
547 25 min) and resuspended in 6 ml CL buffer 2 (100 mM Tris/HCl, 10 mM $MgCl_2$, 1 M NaCl, pH
548 7.5). DNase, protease inhibitor cocktail and phenylmethylsulfonly fluoride were added prior
549 to sonication at low levels before ultracentrifugation of the lysate (140,000 × g, 4°C, 1 h). The
550 membrane pellet was resuspended in 2.5 ml of CL buffer 3 (25 mM Tris/HCl, 10 mM $MgCl_2$, 1
551 M NaCl, 1% Triton X-100, 20% glycerol, pH 7.5) and the solubilised membrane extracted o/n
552 with stirring at 4°C.

553 Samples were ultracentrifuged (140,000 × *g*, 4°C, 1 h) to remove debris, before
554 removing 2 × 1.2 ml of each supernatant to be subsequently diluted with 0.6 ml of CL buffer
555 4 (75 mM Tris/HCl, 10 mM $MgCl_2$, 1 M NaCl, pH 7.5). One sample was incubated with an
556 optimised concentration of specific antibody with the other used as a negative control. Both
557 samples were incubated at 4°C with agitation for 5 h. For the isolation of antibodies, and thus
558 cross-linked interaction partners, 100 µl of protein G-coupled agarose bead resin (Roche)
559 were washed (2 × CL buffer 4, 2 × CL wash buffer [2:1 CL buffer 3 and CL buffer 4]) and added
560 to each sample, and incubated o/n at 4°C with agitation.

561 Samples were centrifuged and the supernatant retained before washing the beads 10
562 × 1 ml with CL wash buffer. After the final wash, beads were resuspended in 250 µl CL wash
563 buffer and transferred to 2 ml spin dry columns and centrifuged to isolate the beads. These
564 were then resuspended in 50 µl of fresh SDS-loading buffer and boiled to elute bound proteins,
565 and reverse cross-linkage, and were collected by centrifugation (10,000 × *g*, RT, 5 min).
566 Supernatant and elution samples were resolved by SDS-PAGE and transferred to a
567 nitrocellulose membrane by Western blotting to detect for specific interaction partners using
568 purified antibodies. The secondary antibody used here is Trueblot Anti-Rabbit IgG-HRP
569 specific for native antibodies.

570 **Peptidoglycan digestion assays**. To test for hydrolase activity on PG, 10 µl of sacculi
571 isolated from strains of interest (usually *E. coli* strains MC1061, BW25113 or D456) were
572 incubated with 1-10 µM of respective enzymes, 37°C for between 1 h and overnight, as
573 indicated for respective proteins. The standard reaction conditions were 10 mM HEPES/NaOH,
574 10 mM $MgCl_2$, 150 mM NaCl, 0.05% Triton X-100, pH 7.5, in 100 µl reaction volume. Following
575 incubation, samples were boiled at 100°C, 10 min, to terminate reactions before digesting
576 remaining PG overnight at 37°C, with 1 µM cellosyl. The samples were centrifuged at 10,000
577 × *g* for 5 min, RT, to obtain digested muropeptide products in the supernatant.

578 To test for activity against soluble muropeptides; first, 100 µl of intact sacculi were
579 incubated overnight at 37°C with 1 µM cellosyl and cellosyl digestion buffer (20 mM $NaPO_4$,
580 pH 4.8). Next, samples were boiled at 100 °C, 10 min, before centrifugation at 10,000 × *g* for
581 5 min, RT, to obtain the soluble muropeptides in the supernatant (87). Ten µl of the
582 supernatant was then used as muropeptide substrate for incubating with enzymes of interest,
583 for the appropriate incubation time, at 37°C. Reactions were then terminated by boiling at
584 100°C for 10 min.

585 After digestion of respective substrates, products were reduced with $NaBH_4$, adjusted
586 to pH 4-5 and separated for analysis by reversed-phase HPLC as described below in HPLC
587 analysis.

588 **Reduction of muropeptides with sodium borohydride.** PG digestion samples were
589 transferred to 2 ml vials following centrifugation. Muropeptides were reduced in a 1:1 volume
590 ratio of sodium borohydride buffer (0.5 M sodium borate, pH 9.0) and a small spatula of
591 sodium borohydride pellets, centrifuging at 3000 × *g,* 30 min, RT as described in (87). The
592 samples were adjusted to pH 4-5 using HPLC grade phosphoric acid before separation and
593 analysis by reversed-phase HPLC.

594 **Reversed-phase HPLC analysis of muropeptides.** Following the protocol of (87),
595 reduced muropeptides were separated for analysis on reversed-phase HPLC systems with a
596 Prontosil 120-3-C18-AQ 3 µm reversed-phase HPLC column (Bischoff). A linear gradient of
597 solvent A (50 mM sodium phosphate, pH 4.31 supplemented with 0.2% NaN_3) to 100 %
598 solvent B (75 mM sodium phosphate, pH 4.95, 15% methanol) over 90 or 180 min was used
599 to separate muropeptides at 52°C. Unlabelled muropeptides were detected at UV absorbance
600 205 nm. In assays where ^{14}C-radiolabelled muropeptides were used, detection was achieved
601 by flowing scintillation cocktail along with standard buffers to give a radioisotope scintillation
602 count (radioactivity CPM). Muropeptide profiles were recorded and analysed using Laura
603 V4.2.11.129 (LabLogic Systems Ltd.).

604 **Spectrophotometric D-alanine release assay (DD-carboxypeptidase assay).** This
605 protocol was adapted from (58). The carboxypeptidase (CPase) activity of PG hydrolases
606 results in the release of the terminal D-Ala residue from the pentapeptide stem of PG
607 precursors. Using UDP-Mur*N*Ac pentapeptide as a substrate, and in this case PBP4, it was
608 possible to spectrophotometrically measure the release of D-Ala.

609 Each reaction sample consisted of 200 µl of CPase buffer (50 mM HEPES/NaOH, 10
610 mM $MgCl_2$, pH 7.6), 3 units of D-amino acid oxidase (Sigma), 6 units of horseradish peroxidase
611 (HRP) (Sigma), Amplex Red (Sigma), and an optimised concentration of protein.

612 All constituents of the reaction were added and mixed directly in a quartz cuvette
613 (Hellma, 10 mM light path, 15 mM centre), before the addition, and brief mixing by pipette,
614 of purified UDP-Mur*N*Ac pentapeptide (BACWAN, Warwick University) to begin the reaction.
615 The released D-Ala residues from the CPase activity of PBP4 are oxidatively deaminated by
616 the action of D-amino acid oxidase to produce pyruvate and hydrogen peroxide (H_2O_2). The
617 released H_2O_2 is reduced to H_2O by HRP using Amplex Red as an electron donor. Oxidised

618 Amplex Red produces resorufin, which has an intense pink colour and the production of which
619 was measured spectrophotometrically using a Cary 100 Bio UV-visible spectrophotometer
620 (wavelength 555 nm). The change in absorption over 10 min was measured and analysed
621 using the complementing software.

622 **Circular dichroism.** Proteins were dialysed overnight against 10 mM $NaPO_4$, pH 7.5
623 and concentrated/diluted to 0.4 mg/ml. CD measurements were taken using a Jasco J-810
624 spectropolarimeter using a wavelength range of 180-250 nm. The average of 10 runs was
625 taken for each protein with a buffer control subtraction. For a direct comparison, correcting
626 for the differing amino acid sequences, the collected data were converted to molecular CD
627 and plotted against wavelength (nm). The resulting CD spectra are compared in Fig. S4 and
628 show that PBP4 lacking domain 3 is folded, consisting of both α-helices (~190, 208 and 222
629 nm) and β-sheets (~210 nm).

630 **Analytical ultracentrifugation.** Purified PBP4 and PBP4ΔD3 were dialyzed over night
631 against 25 mM HEPES/NaOH, 150 mM NaCl, pH 7.5, in preparation for AUC experiments. AUC
632 sedimentation velocity (SV) experiments were carried out in a Beckman Coulter (Palo Alto,
633 CA, USA) ProteomeLab XL-I analytical ultracentrifuge using absorbance at 280 nm and
634 interference detection. The AUC runs were executed at the rotation speed of 45,000 rpm and
635 the temperature of 20°C using an 8-hole AnTi50 rotor and double-sector aluminium-Epon
636 centerpieces. The sample volume was 400 µl and the sample concentrations ranged between
637 approximately 0.25 and 1.4 mg/ml. The partial specific volumes ($\bar{v}$) of the proteins were
638 calculated from their amino acid sequence, using the program SEDNTERP (88). Sedimentation
639 velocity boundaries were analyzed using the size-distribution c(s) model implemented in the
640 program SEDFIT http://www.analyticalultracentrifugation.com (89). The experimental values
641 of the sedimentation coefficient were converted to the standard conditions (s20,w), which is

642 the value of sedimentation coefficient in water at 20°C. The size-distribution peaks were
643 integrated to obtain the weight-averaged values for sedimentation coefficient and molecular
644 mass.

645 The atomic coordinates from the published high-resolution structure of (56) (pdb
646 accession code 2EX2) were used to calculate the sedimentation coefficient values for the
647 monomeric and dimeric forms of PBP4 /PBP4ΔD3 using the program SoMo (90). PBP4
648 /PBP4ΔD3 crystallographic dimer was built using program PyMol (https://pymol.org/2/).

649 **PG binding assay.** To assay for interactions of respective proteins with purified PG, we
650 used a PG binding protocol as described in (91). Briefly, ~100 µg purified PG was pelleted by
651 centrifugation (10,000 × *g,* 10 min, 4°C) and resuspended in binding buffer (10 mM
652 Tris/Maleate, 10 mM $MgCl_2$, 50 mM NaCl, pH 6.8). PG was incubated with 10 µg of desired
653 protein before incubating on ice for 30 min and centrifuging at 10,000 × *g,* 10 min, 4°C. An
654 aliquot of the supernatant (S) was taken for SDS-PAGE. The pelleted PG was washed with 200
655 µl binding buffer by centrifugation as before and the wash supernatant was taken as sample
656 W for SDS-PAGE. The pelleted PG was then resuspended in 100 µl of 2% SDS and incubated
657 for 1 h on a stirring plate, 4°C. Mixtures were centrifuged a final time at 10,000 × *g,* 10 min,
658 4°C, with the supernatant, now containing any initially bound protein, taken as the pellet
659 sample (P). A negative control sample with no PG was assayed in parallel to determine that
660 binding of protein was specific. Samples, along with corresponding controls, were analysed
661 by SDS-PAGE and visualised by Coomassie staining. Presence of protein band in pellet sample
662 (P) indicated binding to PG, whilst presence in supernatant sample (S) indicated no binding.

663 **Bocillin binding assay.** A fluorescent-bocillin binding assay was used to determine
664 whether a PBP was purified with a correctly folded active site. Bocillin FL is a commercially
665 available dye-β-lactam conjugate, synthesised from penicillin V and BODIPY (Molecular

666 Probes, In., Eugene, Oreg.). Ten µg of purified PBP was incubated for 10 min at 37°C, with 20
667 ng of Bocillin FL in a 50 µl volume with 10 mM HEPES/NaOH, 10 mM $MgCl_2$, pH 7.5. A negative
668 control sample was pre-incubated with 1 mM ampicillin for 30 min, 37°C, to block the PBP
669 active site, prior to incubation with Bocillin FL. After incubation, samples were boiled at 100
670 °C for 10 min with 40 µl of SDS-PAGE loading buffer and resolved by SDS-PAGE. Fluorescent
671 signal was observed using Typhoon Fluorescence-imager (Excitation; 488 nm, emission; 520
672 nm, BP20 PMT 400-600 V), followed by visualisation of gels by Coomassie staining. Proteins
673 incubated with ampicillin should have no detectable binding of Bocillin FL. For whole cells, a
674 culture was grown in 5 mL TY and induced with 10 µM IPTG for 3 mass doublings to an OD_{600}
675 of 0.5 and the cells were pelleted and washed once with PBS (8 g NaCl, 1.8 g Na_2HPO_4, 0.24 g
676 KH_2PO_4 per liter, adjusted to pH 7.4) at 4°C and resuspended in 100 µl PBS with 5µg/ml Bocilin
677 FL and incubated for 20 min at RT. To remove the excess Bocillin FL, the samples were pelleted
678 and resuspended in 100 µl PBS with cOmplete™ Mini Protease Inhibitor Cocktail (Sigma) and
679 2 U DNAse I (NEB). Then sonicated on ice for 10 sec and boiled 15' at 99°C after adding 25 µL
680 of SDS-PAGE 5x loading buffer and resolved by SDS-PAGE. Fluorescent signal was observed
681 using a home-made imager for Midori green, followed by visualisation of gels by Coomassie
682 staining.

683 ***In vitro* PG synthesis assay with radiolabelled lipid II.** The assay was published by
684 Bertsche et al., (92). Lipid II (1.2 nmol, 11,000 dpm) was vacuum dried and dissolved in 5 µl of
685 methanol. The reaction was performed in a total volume of 50 µl in 25 mM Tris/HCl, 10 mM
686 $MgCl_2$, 100 mM NaCl, 0.05% Triton X-100, pH 7.5 (buffer B), with 0.5 µM PBP1A, 1 µM LpoA,
687 1 µM PBP4(S62A), 2 µM NlpI. The reaction was performed for 1 h at 30°C. The pH of the
688 samples was adjusted to 4.8 prior to boiling for 5 min followed by a digestion with 50 g/ml
689 cellosyl for 1 h at 37°C and boiling for 5 min.

690

691 **ACKNOWLEDGEMENTS**

692 We thank David Roper and Smita Chauhan (University of Warwick) for help with the
693 carboxypeptidase assay, Helen Waller (Newcastle University) for help with circular dichroism
694 methodology, and Lisa Atkinson and Daniela Vollmer (Newcastle University) for preparation
695 of PG sacculi. The work was supported by funding from the Wellcome Trust (101824/Z/13/Z),
696 to WV). X.L. was supported by the China Scholarship Council fellowship (File
697 No.201406220123).

698 J.V., A.L., H.C.L.Y, X.L., A.S.S., and M.B did most experiments. A.T., M.B., V.W., and T.B.
699 designed most experiments. M.B, W.V and TdB analyzed the data and wrote the manuscript.
700 All authors critically read the manuscript and provided feedback.

701

702 **TABLE 1 Strain and plasmids used in this study.**

Strain	Mutation	Genotype	Source
LMC500 (MC4100)	Wild-type	F^-, *araD139, Δ(argF-lac)U169, deoC1, flbB5301, lysA1, ptsF25, rbsR, relA1, rpsL150*	(80)
BL21(DE3)	Overexpression strain	F^- *ompT, dcm lon hsdS hsdSB(rB-mB-)* λ(DE3)	Novagen
BW25113	Keio background strain	*F^-, DE(araD-araB)567, lacZ4787(del)::rrnB-3, LAM-, rph-1, DE(rhaD-rhaB)568, hsdR514*	(77)
DH5α	Storage strain	F^- *endA1 glnV44 thi-1 recA1* φ80Δ*lacZ*ΔM15, $λ^-$	Invitrogen
MC1061	Laboratory strain	Δ(*araA-leu*)7697 Δ(*lac*)X74 *galK*16 *galE*15(GalS) $λ^-$e14- *mcrA*0 *relA1 rpsL*150(str^R) *spoT1 mcrB1 hsdR2*	(93)
LMC509	FtsZ (ts)	MC4100 *ftsZ*184	(80)
LMC511	FtsA (ts)	MC4100 *ftsA*10	(80)
LMC512	FtsA (ts)	MC4100 *ftsA*1882	(80)
LMC515	FtsE (ts)	MC4100 *ftsE*1181	(80)
LMC531	FtsQ (ts)	MC4100 *ftsQ*(ts)	(80)

LMC2487	FtsW (ts)	JLB17; F^- *thr, trp, his, thy, ara, lac, gal, xyl, mtl, rspL, tonA*, *ftsW* amino acid replacement G311D	(94)
LMC510	PBP3 (ts)	MC4100 *ftsI* 2158	(80)
BCB677	ΔPBP1A	BW25113Δ*mrcA*	(95)
BCB678	ΔPBP1B	BW25113Δ*mrcB*	(95)
BCB192	ΔLpoA	BW25113Δ*lpoA*	(95)
LMC2217	ΔLpoB	BW25113Δ*lpoA*	(95)
BCB655	ΔPBP4	BW25113Δ*dacB*	(95)
BCB904	ΔNlpI	BW25113Δ*nlpI*	(95)
BCB1363	ΔPBP4ΔLpoA	BW25113Δ*dacB:kan*^{R}, Δ*lpoA*	This work
BCB744	ΔFtsE	BW25113Δ*ftsE* kan^R CAG60397	This work
BCB746	ΔFtsEX	BW25113Δ*ftsE*X cat^R CAG60399	This work
BCB1081	ΔFtsE 1-150	XL34 LMC500Δ*fts*E 1-150::*kan-fts*X	This work
BCB849	ΔFtsE 1-150	XL35 LMC500Δ*fts*E 1-150::*fts*X	This work
BCB1082	ΔFtsE	XL33 LMC500Δ*fts*E::-cam-p*Trc99A*down *fts*X	This work
BCB850	ΔFtsE	XL36 LMC500Δ*fts*E::p*Trc99A*down *fts*X	This work

Plasmid	Name	Characteristics	Source
pET21b	pET21b-PBP4(S62A)Δ1-60	Inactive PBP4 lacking residues 1-60 (Amp^R)	(3)
pET21b	pET21b-His-PBP4(S62A)Δ1-60	For purification of His-PBP4 (active site mutant) (Amp^R)	(3)
pET21b	pET21b-PBP4Δ1-60	Native PBP4 lacking residues 1-60 (Amp^R)	(3)
pET28a	pET28a-His-LpoA(sol)	Soluble LpoA (LpoAΔ1-27) construct, N-terminal His-tag, Kan^R	(66)
pET28a	pET28-His-LpoA^N	Purification of His-LpoA^N	(66)
pET28a	pET28-His-LpoA^C	Purification of His-LpoA^C	(66)
pTK1A-His	pTK1A-His	Full length His-PBP1A, Kan^R	(66)
pET28a-	pET28a-His-NlpI	Soluble NlpI construct, N-terminal His-tag, KanR	(6)
pBAD18	pBAD18-His-PBP4ΔD3	for purification of His- PBP4 lacking domain 3 (Amp^R)	This work
pXL86	pTHV mCh-FtsE wt	p*Trc* 99A down expressing mCh-FtsE(wt) colE1 ori, Amp^R	This work
pXL89	pTHV mCh-FtsE ts	p*Trc* 99A down expressing mCh-FtsE(ts) (P135S) colE1 ori, Amp^R	This work
pXL110	pSAV mNG-NNN-FtsE	p*Trc* 99A down expressing mNG-FtsE, p15A origin, Cam^R	This work
pXL133	pSAV-PBP4	p*Trc* 99A down expressing PBP4, p15A origin, Cam^R	This work

pXL134	pSAV-PBP4 S62G	p*Trc* 99A down expressing PBP4 S62G, p15A origin, Cam^R	This work
pXL135	pSAV-FtsE	p*Trc* 99A down expressing FtsE, p15A origin, Cam^R	This work
pXL136	pSAV-FtsE(ts)	p*Trc* 99A down expressing FtsE(ts), p15A origin, Cam^R	This work
pXL137	pSAV-FtsE K41Q	p*Trc* 99A down expressing FtsE K41Q, p15A origin, Cam^R	This work
pXL138	pSAV-FtsE D162A	p*Trc* 99A down expressing FtsE D162A, p15A origin, Cam^R	This work
pXL139	pSAV-FtsE E163A	p*Trc* 99A down expressing FtsE E163A, p15A origin, Cam^R	This work
pXL140	pSAV-PBP4-ΔD3	p*Trc* 99A down expressing PBP4Δ173-247 (domain 3), p15A origin, Cam^R	This work
pXL150	pSAV-PBP4-D155A	p*Trc* 99A down expressing PBP4 D155A, p15A origin, Cam^R	This work
pXL151	pSAV-PBP4-R361A	p*Trc* 99A down expressing PBP4 DR361A, p15A origin, Cam^R	This work

TABLE 2 Primers used in this study.

Primer	Sequence 5'-3'	Purpose
priXL51	ACCATGGCTAATTCCCATGTCAG	GA_pkd3_F
priXL54	GTGTAGGCTGGAGCTGCTTC	PCR_pkd3_R
priXL187	CCGGCCGAATTCAACAACAACTCGATGATTCGCTTTGAACATG TCAGC	FtsE-EcoRI fw
priXL188	GGCCAAGCTTTTATTCATGGCCCACGCCTCC	FtsE-EcoRI rv
priXL221	CATGAAGCCGTTGGCTTAACC	ΔFtsE-FA-F
priXL222	TAGGAACTTCGAAGCAGCTCCAGCCTACACTGTTAATCCTCTC GGGCAAAAAG	ΔFtsE -FA-R
priXL223	GGATATTCATATGGACCATGGCTAATTCCCATGTCAGGCGGT GGTGAACAAGCCCGC	ΔFtsE- 1-150
priXL224	GGTGAGCATGCGATAGGAACG	ΔFtsE-1:150
priXL225	TGAGCGGATAACAATTTCACACAGGAAACAGACCATGAATAA GCGCGATGCAATC	ΔFtsE-clean
priXL226	CTTTTCAGATCCTGCAATGCG	ΔFtsE-clean
priXL230	ATTCCGGCGCAGGGCAAAGTACTCTCCTGAAGCTG	FtsE-K41Q-F
priXL231	GATCAGCTTCAGGAGAGTACTTTGCCCTGCGCCGGA	FtsE-K41Q-R

priXL232	CGGTACTGCTAGCGGCTGAACCGACTGGTAACCTG	FtsE-D162A-F
priXL233	AGGTTACCAGTCGGTTCAGCCGCTAGCAGTACCGC	FtsE-D162A-R
priXL234	GTACTGCTAGCGGACGCTCCGACTGGTAACCT	FtsE-E163A-F
priXL235	AGGTTACCAGTCGGAGCGTCCGCTAGCAGTACCGC	FtsE-E163A-R
priXL236	AGATGGCGCTGCCTGCCGGCACCCAGAAAG	PBP4-S62G-F
priXL244	GCGCGAATTCatgCGATTTTCCAGATTTATCA	EcoRI-PBP4-F
priXL245	GCGCAAGCTTctaATTGTTCTGATAAATATC	HindIII-PBP4-R
priXL250	GTTGACCGCAACGGTGGCGGAAGCGGGTCTGTGCAGGATGGAGCCAGCTATG	PBP4ΔD3-F
priXL251	TCCATCCTGCACAGACCCGCTTCCGCCACCGTTGCGGTCAACTATGGCGGC	PBPΔD3-R
priXL266	CCGGCTGGCCATGGAATGCCATGACACAATGCTTTAGCGCTC	PBP4-D155A-F
priXL267	GGAGCGCTAAAGCATTGTGTCATGGCATTCCATGGCCAGCCGG	PBP4-D155A-R
priXL268	GCCGATGGTTCAGGGCTTTCGGCGCATAACCTGATTGCCCCCGCC	PBP4-R361A-F
priXL269	GGCGGGGGCAATCAGGTTATGCGCCGAAAGCCCTGAACCATCGGC	PBP4-R361A-R

REFERENCES

1. Vollmer W, Blanot D, De Pedro MA. 2008. Peptidoglycan structure and architecture 32:149–167.

2. Egan AJF, Errington J, Vollmer W. 2020. Regulation of peptidoglycan synthesis and remodelling. Nat Rev Micro 18:446–460.

3. Banzhaf M, Yau HCL, Verheul J, Lodge A, Kritikos G, Mateus A, Cordier B, Hov A-K, Stein F, Wartel M, Pazos M, Solovyova AS, Breukink E, van Teeffelen S, Savitski MM, Blaauwen den T, Typas A, Vollmer W. 2020. Outer membrane lipoprotein NlpI scaffolds peptidoglycan hydrolases within multi-enzyme complexes in *Escherichia coli*. EMBO J e102246.

4. Gray AN, Egan AJ, Van't Veer IL, Verheul J, Colavin A, Koumoutsi A, Biboy J, Altelaar AFM, Damen MJ, Huang KC, Simorre J-P, Breukink E, Blaauwen den T, Typas A, Gross CA, Vollmer W. 2015. Coordination of peptidoglycan synthesis and outer membrane constriction during Escherichia coli cell division. Elife (Cambridge) 4. 0.7554/eLife.07118.

5. Bertsche U, Kast T, Wolf B, Fraipont C, Aarsman MEG, Kannenberg K, Rechenberg von M, Nguyen-Distèche M, Blaauwen den T, Höltje J-V, Vollmer W. 2006. Interaction between two murein (peptidoglycan) synthases, PBP3 and PBP1B, in *Escherichia coli*. Mol Microbiol 61:675–690.

6. Born P, Breukink E, Vollmer W. 2006. In vitro synthesis of cross-linked murein and its attachment to sacculi by PBP1A from *Escherichia coli.* J Biol Chem 281:26985–26993.

731 7. Egan AJF, Biboy J, van't Veer I, Breukink E, Vollmer W. 2015. Activities and regulation
732 of peptidoglycan synthases. Philos Trans R Soc Lond, B, Biol Sci 370.

733 8. Rohs PDA, Buss J, Sim SI, Squyres GR, Srisuknimit V, Smith M, Cho H, Sjodt M, Kruse
734 AC, Garner EC, Walker S, Kahne DE, Bernhardt TG. 2018. A central role for PBP2 in the
735 activation of peptidoglycan polymerization by the bacterial cell elongation machinery.
736 PLoS Genet 14:e1007726.

737 9. Meeske AJ, Riley EP, Robins WP, Uehara T, Mekalanos JJ, Kahne D, Walker S, Kruse
738 AC, Bernhardt TG, Rudner DZ. 2016. SEDS proteins are a widespread family of
739 bacterial cell wall polymerases. Nature 537:634–638.

740 10. Taguchi A, Welsh MA, Marmont LS, Lee W, Sjodt M, Kruse AC, Kahne D, Bernhardt TG,
741 Walker S. 2019. FtsW is a peptidoglycan polymerase that is functional only in complex
742 with its cognate penicillin-binding protein. Nature Microbiology 2:a000414.

743 11. van der Ploeg R, Verheul J, Vischer NOE, Alexeeva S, Hoogendoorn E, Postma M,
744 Banzhaf M, Vollmer W, Blaauwen den T. 2013. Colocalization and interaction
745 between elongasome and divisome during a preparative cell division phase in
746 *Escherichia coli*. Mol Microbiol 87:1074–1087.

747 12. Datta P, Dasgupta A, Singh AK, Mukherjee P, Kundu M, Basu J. 2006. Interaction
748 between FtsW and penicillin-binding protein 3 (PBP3) directs PBP3 to mid-cell,
749 controls cell septation and mediates the formation of a trimeric complex involving
750 FtsZ, FtsW and PBP3 in mycobacteria. Mol Microbiol 62:1655–1673.

751 13. Fraipont C, Alexeeva S, Wolf B, van der Ploeg R, Schloesser M, Blaauwen den T,
752 Nguyen-Distèche M. 2011. The integral membrane FtsW protein and peptidoglycan
753 synthase PBP3 form a subcomplex in *Escherichia coli.* Microbiology 157:251–259.

754 14. Pazos M, Peters K, Vollmer W. 2017. Robust peptidoglycan growth by dynamic and
755 variable multi-protein complexes. Curr Opin Microbiol 36:55–61.

756 15. Sarkar SK, Dutta M, Chowdhury C, Kumar A, Ghosh AS. 2011. PBP5, PBP6 and DacD
757 play different roles in intrinsic -lactam resistance of *Escherichia coli*. Microbiology
758 (Reading, Engl) 157:2702–2707.

759 16. Potluri L, Karczmarek A, Verheul J, Piette A, Wilkin J-M, Werth N, Banzhaf M, Vollmer
760 W, Young KD, Nguyen-Distèche M, Blaauwen den T. 2010. Septal and lateral wall
761 localization of PBP5, the major D,D-carboxypeptidase of *Escherichia coli,* requires
762 substrate recognition and membrane attachment. Mol Microbiol 77:300–323.

763 17. Hugonnet J-E, Mengin-Lecreulx D, Monton A, Blaauwen den T, Carbonnelle E,
764 Veckerlé C, Brun Y, van Nieuwenhze M, Bouchier C, Tu K, Rice LB, Arthur M. 2016.
765 Factors essential for L,D-transpeptidase-mediated peptidoglycan cross-linking and β-
766 lactam resistance in *Escherichia coli*. Elife (Cambridge) 5:2006.

767 18. Meiresonne NY, van der Ploeg R, Hink MA, Blaauwen den T. 2017. Activity-Related
768 Conformational Changes in d,d-Carboxypeptidases Revealed by In Vivo Periplasmic
769 Förster Resonance Energy Transfer Assay in *Escherichia coli*. mBio 8:e01089–17.

770 19. Peters K, Kannan S, Rao VA, Biboy J, Vollmer D, Erickson SW, Lewis RJ, Young KD,
771 Vollmer W. 2016. The Redundancy of Peptidoglycan Carboxypeptidases Ensures
772 Robust Cell Shape Maintenance in *Escherichia coli*. mBio 7. 00819-16

773 20. Singh SK, Saisree L, Amrutha RN, Reddy M. 2012. Three redundant murein
774 endopeptidases catalyse an essential cleavage step in peptidoglycan synthesis of
775 *Escherichia coli* K12. Mol Microbiol 86:1036–1051.

776 21. Meberg BM, Paulson AL, Priyadarshini R, Young KD. 2004. Endopeptidase penicillin-
777 binding proteins 4 and 7 play auxiliary roles in determining uniform morphology of
778 *Escherichia coli*. J Bacteriol 186:8326–8336.

779 22. Peters NT, Dinh T, Bernhardt TG. 2011. A fail-safe mechanism in the septal ring
780 assembly pathway generated by the sequential recruitment of cell separation
781 amidases and their activators. J Bacteriol 193:4973–4983.

782 23. Heidrich C, Templin MF, Ursinus A, Merdanovic M, Berger J, Schwarz H, De Pedro MA,
783 Höltje JV. 2001. Involvement of N-acetylmuramyl-L-alanine amidases in cell
784 separation and antibiotic-induced autolysis of *Escherichia coli*. Mol Microbiol 41:167–
785 178.

786 24. Bernhardt TG, De Boer PAJ. 2003. The *Escherichia coli* amidase AmiC is a periplasmic
787 septal ring component exported via the twin-arginine transport pathway. Mol
788 Microbiol 48:1171–1182.

789 25. Uehara T, Parzych KR, Dinh T, Bernhardt TG. 2010. Daughter cell separation is
790 controlled by cytokinetic ring-activated cell wall hydrolysis. EMBO J 29:1412–1422.

791 26. van Straaten KE, Dijkstra BW, Vollmer W, Thunnissen A-MWH. 2005. Crystal structure
792 of MltA from *Escherichia coli* reveals a unique lytic transglycosylase fold. J Mol Biol
793 352:1068–1080.

794 27. van Heijenoort J. 2011. Peptidoglycan hydrolases of *Escherichia coli.* Microbiol Mol
795 Biol Rev 75:636–663.

796 28. Yunck R, Cho H, Bernhardt TG. 2015. Identification of MltG as a potential terminase
797 for peptidoglycan polymerization in bacteria. Mol Microbiol.

798 29. Raychaudhuri D. 1999. ZipA is a MAP-Tau homolog and is essential for structural
799 integrity of the cytokinetic FtsZ ring during bacterial cell division. EMBO J 18:2372–
800 2383.

801 30. Pazos M, Peters K, Casanova M, Palacios P, VanNieuwenhze M, Breukink E, Vicente
802 M, Vollmer W. 2018. Z-ring membrane anchors associate with cell wall synthases to
803 initiate bacterial cell division. Communications 9:5090–12.

804 31. Galli E, Gerdes K. 2012. FtsZ-ZapA-ZapB Interactome of *Escherichia coli*. J Bacteriol
805 194:292–302.

806 32. Durand-Heredia JM, Yu HH, De Carlo S, Lesser CF, Janakiraman A. 2011. Identification
807 and Characterization of ZapC, a Stabilizer of the FtsZ Ring in *Escherichia coli*. J
808 Bacteriol 193:1405–1413.

809 33. Hale CA, Shiomi D, Liu B, Bernhardt TG, Margolin W, Niki H, De Boer PAJ. 2011.
810 Identification of *Escherichia coli* ZapC (YcbW) as a component of the division
811 apparatus that binds and bundles FtsZ polymers. J Bacteriol 193:1393–1404.

812 34. Roach EJ, Wroblewski C, Seidel L, Berezuk AM, Brewer D, Kimber MS, Khursigara CM.
813 2016. Structure and Mutational Analysis of *Escherichia coli* ZapD Reveals Charged
814 Residues Involved in FtsZ Filament Bundling. J Bacteriol. 198: 1683-1693.

815 35. Marteyn BS, Karimova G, Fenton AK, Gazi AD, West N, Touqui L, Prévost M-C, Betton
816 J-M, Poyraz O, Ladant D, Gerdes K, Sansonetti PJ, Tang CM. 2014. ZapE is a novel cell
817 division protein interacting with FtsZ and modulating the Z-ring dynamics. mBio
818 5:e00022–14.

819 36. Du S, Pichoff S, Lutkenhaus J. 2016. FtsEX acts on FtsA to regulate divisome assembly
820 and activity. Proc Natl Acad Sci USA 113:E5052–61.

821 37. Corbin BD, Wang Y, Beuria TK, Margolin W. 2007. Interaction between Cell Division
822 Proteins FtsE and FtsZ. J Bacteriol 189:3026–3035.

823 38. Priyadarshini R, Popham DL, Young KD. 2006. Daughter Cell Separation by Penicillin-
824 Binding Proteins and Peptidoglycan Amidases in *Escherichia coli.* J Bacteriol
825 188:5345–5355.

826 39. Yang DC, Peters NT, Parzych KR, Uehara T, Markovski M, Bernhardt TG. 2011. An ATP-
827 binding cassette transporter-like complex governs cell-wall hydrolysis at the bacterial
828 cytokinetic ring. Proc Natl Acad Sci USA 108:E1052–60.

829 40. Yang DC, Tan K, Joachimiak A, Bernhardt TG. 2012. A conformational switch controls
830 cell wall-remodelling enzymes required for bacterial cell division. Mol Microbiol
831 85:768–781.

832 41. Tsang M-J, Yakhnina AA, Bernhardt TG. 2017. NlpD links cell wall remodeling and
833 outer membrane invagination during cytokinesis in *Escherichia coli*. PLoS Genet
834 13:e1006888.

835 42. Aarsman MEG, Piette A, Fraipont C, Vinkenvleugel TMF, Nguyen-Distèche M,
836 Blaauwen den T. 2005. Maturation of the *Escherichia coli* divisome occurs in two
837 steps. Mol Microbiol 55:1631–1645.

838 43. Gamba P, Veening J-W, Saunders NJ, Hamoen LW, Daniel RA. 2009. Two-step
839 assembly dynamics of the *Bacillus subtilis* divisome. J Bacteriol 191:4186–4194.

840 44. Perez AJ, Cesbron Y, Shaw SL, Bazan Villicana J, Tsui H-CT, Boersma MJ, Ye ZA,
841 Tovpeko Y, Dekker C, Holden S, Winkler ME. 2019. Movement dynamics of divisome
842 proteins and PBP2x:FtsW in cells of *Streptococcus pneumoniae*. Proc Natl Acad Sci
843 USA 116:3211–3220.

844 45. Monteiro JM, Pereira AR, Reichmann NT, Saraiva BM, Fernandes PB, Veiga H, Tavares
845 AC, Santos M, Ferreira MT, Macário V, VanNieuwenhze MS, Filipe SR, Pinho MG.
846 2018. Peptidoglycan synthesis drives an FtsZ-treadmilling-independent step of
847 cytokinesis. Nature 554:528–532.

848 46. Tsang M-J, Bernhardt TG. 2015. A role for the FtsQLB complex in cytokinetic ring
849 activation revealed by an *ftsL* allele that accelerates division. Mol Microbiol 95:925–
850 944.

851 47. Tsang M-J, Bernhardt TG. 2014. A role for the FtsQLB complex in cytokinetic ring
852 activation revealed by an *ftsL* allele that accelerates division. Mol Microbiol.

853 48. Bernard CS, Sadasivam M, Shiomi D, Margolin W. 2007. An altered FtsA can
854 compensate for the loss of essential cell division protein FtsN in *Escherichia coli*. Mol
855 Microbiol 64:1289–1305.

856 49. Boes A, Olatunji S, Breukink E, Terrak M. 2019. Regulation of the peptidoglycan
857 polymerase activity of PBP1b by antagonist actions of the core divisome Proteins
858 FtsBLQ and FtsN. mBio 10:e01912–18.

859 50. Blaauwen den T, Luirink J, 2019. Checks and Balances in Bacterial Cell Division. mBio.
860 e00149-19

861 51. Korat B, Mottl H, Keck W. 1991. Penicillin-binding protein 4 of *Escherichia coli*:
862 molecular cloning of the *dacB* gene, controlled overexpression, and alterations in
863 murein composition. Mol Microbiol 5:675–684.

864 52. Harris F, Brandenburg K, Seydel U. 2002. Investigations into the mechanisms used by
865 the C-terminal anchors of *Escherichia coli* penicillin-binding proteins 4, 5, 6 and 6b for
866 membrane interaction. European Journal of ….

867 53. De Pedro MA, Schwarz U. 1981. Heterogeneity of newly inserted and preexisting
868 murein in the sacculus of *Escherichia coli.* Proc Natl Acad Sci USA 78:5856–5860.

869 54. Iwaya M, Strominger JL. 1977. Simultaneous deletion of D-alanine carboxypeptidase
870 IB-C and penicillin-binding component IV in a mutant of *Escherichia coli* K12. Proc Natl
871 Acad Sci USA 74:2980–2984.

872 55. Nelson DE, Young KD. 2001. Contributions of PBP 5 and DD-carboxypeptidase
873 penicillin binding proteins to maintenance of cell shape in *Escherichia coli.* J Bacteriol
874 183:3055–3064.

875 56. Kishida H, Unzai S, Roper DI, Lloyd A, Park S-Y, Tame JRH. 2006. Crystal Structure of
876 Penicillin Binding Protein 4 (dacB) from *Escherichia coli,* both in the Native Form and
877 Covalently Linked to Various Antibiotics †. Biochemistry 45:783–792.

878 57. Thunnissen MMGM, Fusetti F, De Boer B, Dijkstra BW. 1995. Purification,
879 crystallisation and preliminary X-ray analysis of penicillin binding protein 4 from
880 *Escherichia coli*, a protein related to class a β-lactamases. J Mol Biol 247:149–153.

881 58. Clarke TB, Kawai F, Park S-Y, Tame JRH, Dowson CG, Roper DI. 2009. Mutational
882 analysis of the substrate specificity of *Escherichia coli* penicillin binding protein 4.
883 Biochemistry 48:2675–2683.

884 59. Hocking J, Priyadarshini R, Takacs CN, Costa T, Dye NA, Shapiro L, Vollmer W, Jacobs-
885 Wagner C. 2012. Osmolality-Dependent Relocation of Penicillin-Binding Protein PBP2
886 to the Division Site in *Caulobacter crescentus*. J Bacteriol 194:3116–3127.

887 60. Liu X, Meiresonne NY, Bouhss A, Blaauwen den T. 2018. FtsW activity and lipid II
888 synthesis are required for recruitment of MurJ to midcell during cell division in
889 Escherichia coli. Mol Microbiol 109:855–884.

890 61. Alcorlo M, Dik DA, De Benedetti S, Mahasenan KV, Lee M, Domínguez-Gil T, Hesek D,
891 Lastochkin E, López D, Boggess B, Mobashery S, Hermoso JA. 2019. Structural basis of
892 denuded glycan recognition by SPOR domains in bacterial cell division. Nature
893 Communications 10:5567–13.

894 62. Sykes RB, Bonner DP, Bush K, Georgopapadakou NH. 1982. Azthreonam (SQ 26,776),
895 a synthetic monobactam specifically active against aerobic gram-negative bacteria.
896 Antimicrob Agents Chemother 21:85–92.

897 63. Nanninga N. 1991. Cell division and peptidoglycan assembly in *Escherichia coli*. Mol
898 Microbiol 5:791–795.

899 64. De Pedro MA, Quintela JC, Höltje JV, Schwarz H. 1997. Murein segregation in
900 *Escherichia coli*. J Bacteriol 179:2823–2834.

901 65. Potluri L-P, Kannan S, Young KD. 2012. ZipA is required for FtsZ-dependent preseptal
902 peptidoglycan synthesis prior to invagination during cell division. J Bacteriol
903 194:5334–5342.

904 66. Jean NL, Bougault CM, Lodge A, Derouaux A, Callens G, Egan AJF, Ayala I, Lewis RJ,
905 Vollmer W, Simorre J-P. 2014. Elongated structure of the outer-membrane activator
906 of peptidoglycan synthesis LpoA: implications for PBP1A stimulation. Structure
907 22:1047–1054.

908 67. Jean NL, Bougault C, Derouaux A, Callens G, Vollmer W, Simorre J-P. 2015. Backbone
909 and side-chain (1)H, (13)C, and (15)N NMR assignments of the N-terminal domain of
910 *Escherichia coli* LpoA. Biomol NMR Assign 9:65–69.

911 68. Typas A, Banzhaf M, van den Berg van Saparoea B, Verheul J, Biboy J, Nichols RJ,
912 Zietek M, Beilharz K, Kannenberg K, Rechenberg von M, Breukink E, Blaauwen den T,
913 Gross CA, Vollmer W. 2010. Regulation of peptidoglycan synthesis by outer-
914 membrane proteins. Cell 143:1097–1109.

915 69. Goehring NW, Beckwith J. 2005. Diverse paths to midcell: assembly of the bacterial
916 cell division machinery. Curr Biol 15:R514–26.

917 70. Blaauwen den T, Hamoen LW, Levin PA. 2017. The divisome at 25: the road ahead.
918 Curr Opin Microbiol 36:85–94.

919 71. Pichoff S, Du S, Lutkenhaus J. 2018. Disruption of divisome assembly rescued by FtsN-
920 FtsA interaction in *Escherichia coli*. Proc Natl Acad Sci USA 115:E6855–E6862.

921 72. Du S, Henke W, Pichoff S, Lutkenhaus J. 2019. How FtsEX localizes to the Z ring and
922 interacts with FtsA to regulate cell division. Mol Microbiol.

923 73. Arends SJR, Kustusch RJ, Weiss DS. 2009. ATP-binding site lesions in FtsE impair cell
924 division. J Bacteriol 191:3772–3784.

925 74. Zoghbi ME, Fuson KL, Sutton RB, Altenberg GA. 2012. Kinetics of the
926 association/dissociation cycle of an ATP-binding cassette nucleotide-binding domain.
927 J Biol Chem 287:4157–4164.

928 75. Rice P, Longden I, Bleasby A. 2000. EMBOSS: the European Molecular Biology Open
929 Software Suite. Trends Genet 16:276–277.

930 76. Vischer NOE, Verheul J, Postma M, van den Berg van Saparoea B, Galli E, Natale P,
931 Gerdes K, Luirink J, Vollmer W, Vicente M, Blaauwen den T. 2015. Cell age dependent
932 concentration of *Escherichia coli* divisome proteins analyzed with ImageJ and ObjectJ.
933 Front Microbiol 6:586.

934 77. Datsenko KA, Wanner BL. 2000. One-step inactivation of chromosomal genes in
935 *Escherichia coli* K-12 using PCR products. Proc Natl Acad Sci USA 97:6640–6645.

936 78. Chen JC, Weiss DS, Ghigo JM, Beckwith J. 1999. Septal localization of FtsQ, an
937 essential cell division protein in *Escherichia coli*. J Bacteriol 181:521–530.

938 79. Alexeeva S, Gadella TWJ, Verheul J, Verhoeven GS, Blaauwen den T. 2010. Direct
939 interactions of early and late assembling division proteins in *Escherichia coli* cells
940 resolved by FRET. Mol Microbiol 77:384–398.

941 80. Taschner PE, Huls PG, Pas E, Woldringh CL. 1988. Division behavior and shape
942 changes in isogenic *ftsZ, ftsQ, ftsA, pbpB*, and *ftsE* cell division mutants of *Escherichia*
943 *coli* during temperature shift experiments. J Bacteriol 170:1533–1540.

944 81. Gibson DG, Young L, Chuang R-Y, Venter JC, Hutchison CA, Smith HO. 2009. Enzymatic
945 assembly of DNA molecules up to several hundred kilobases. Nat Chem Biol 6:343–
946 345.

947 82. Buddelmeier N, Aarsman MEG, Blaauwen den T. 2013. Immunolabeling of Proteins in
948 Situ in *Escherichia coli* K12 Strains. bio-protocoll 1–4.

949 83. Koppelman C-M, Aarsman MEG, Postmus J, Pas E, Muijsers AO, Scheffers D-J,
950 Nanninga N, Blaauwen den T. 2004. R174 of *Escherichia coli* FtsZ is involved in
951 membrane interaction and protofilament bundling, and is essential for cell division.
952 Mol Microbiol 51:645–657.

953 84. Ludwig C. 1856. Diffusion between unequally heated regions of initially uniform
954 solutions. Sitzungsber Akad Wiss Wien Math-Naturwiss 20:593.

955 85. Jerabek-Willemsen M, Wienken CJ, Braun D, Baaske P, Duhr S. 2011. Molecular
956 interaction studies using microscale thermophoresis. Assay Drug Dev Technol 9:342–
957 353.

958 86. Müller P, Ewers C, Bertsche U, Anstett M, Kallis T, Breukink E, Fraipont C, Terrak M,
959 Nguyen-Distèche M, Vollmer W. 2007. The essential cell division protein FtsN
960 interacts with the murein (peptidoglycan) synthase PBP1B in *Escherichia coli*. J Biol
961 Chem 282:36394–36402.

962 87. Glauner B, Höltje JV, Schwarz U. 1988. The composition of the murein of *Escherichia*
963 *coli*. J Biol Chem 263:10088–10095.

964 88. laue T, Shah B, Ridgeway T, Pelletier S. 1992. Computer-aided interpretation of
965 analytical sedimentation data for proteins. The Royal Society of Chemistry 90:125.

966 89. Schuck P. 2000. Size-distribution analysis of macromolecules by sedimentation
967 velocity ultracentrifugation and lamm equation modeling. Biophys J 78:1606–1619.

968 90. Brookes E, Demeler B, Rosano C, Rocco M. 2010. The implementation of SOMO
969 (SOlution MOdeller) in the UltraScan analytical ultracentrifugation data analysis suite:
970 enhanced capabilities allow the reliable hydrodynamic modelling of virtually any kind
971 of biomacromolecule. Eur Biophys J 39:423–435.

972 91. Ursinus A, van den Ent F, Brechtel S, de Pedro M, Höltje J-V, Löwe J, Vollmer W. 2004.
973 Murein (peptidoglycan) binding property of the essential cell division protein FtsN
974 from *Escherichia coli*. J Bacteriol 186:6728–6737.

975 92. Bertsche U, Breukink E, Kast T, Vollmer W. 2005. In vitro murein peptidoglycan
976 synthesis by dimers of the bifunctional transglycosylase-transpeptidase PBP1B from
977 *Escherichia coli*. J Biol Chem 280:38096–38101.

978 93. Casadaban MJ, Cohen SN. 1980. Analysis of gene control signals by DNA fusion and
979 cloning in *Escherichia coli*. J Mol Biol 138:179–207.

980 94. Ishino F, Jung HK, Ikeda M, Doi M, Wachi M, Matsuhashi M. 1989. New mutations *fts*-
981 36, *lts*-33, and *ftsW* clustered in the mra region of the *Escherichia coli* chromosome
982 induce thermosensitive cell growth and division. J Bacteriol 171:5523–5530.

983 95. Baba T, Ara T, Hasegawa M, Takai Y, Okumura Y, Baba M, Datsenko KA, Tomita M,
984 Wanner BL, Mori H. 2006. Construction of *Escherichia coli* K-12 in-frame, single-gene
985 knockout mutants: the Keio collection. Mol Syst Biol 2:2006.0008.

986

Midcell localization of PBP4 of *Escherichia coli* is essential for the timing of divisome assembly

Jolanda Verheul[1#], Adam Lodge[2,7#], Hamish C.L. Yau[2,8#], Xiaolong Liu[1,9#], Alexandra S. Solovyova[3], Athanasios Typas[4,5] Manuel Banzhaf[6*], Waldemar Vollmer[2**], and Tanneke den Blaauwen[1***]

[1]Bacterial Cell Biology, Swammerdam Institute for Life Sciences, Faculty of Science, University of Amsterdam; Science Park 904, 1098 XH Amsterdam, The Netherlands.
[2]Centre for Bacterial Cell Biology, Biosciences Institute, Newcastle University, Newcastle upon Tyne, NE2 4AX, United Kingdom.
[3]NUPPA, Leech Building, Framlington Place, Newcastle upon Tyne NE2 4HH, UK
[4]European Molecular Biology Laboratory, Genome Biology Unit, Heidelberg, Germany
[5]European Molecular Biology Laboratory, Structural & Computational Unit, Heidelberg, Germany
[6]Institute of Microbiology & Infection and School of Biosciences, University of Birmingham, Edgbaston, Birmingham, UK. B15 2TT
[7]Present address: Iksuda Therapeutics, The Biosphere, Draymans Way, Newcastle Helix, Newcastle upon Tyne, NE4 5BX, UK
[8]Pressent address: Procter & Gamble, Newcastle Innovation Centre, Whitley Road, Newcastle-Upon Tyne, NE12 9TS, UK.
[9]Department of Biochemistry, University of Oxford, OX1 3QU, Oxford, United Kingdom.

[#]contributed equally.
*Corresponding author. Tel: +44 121 4145586; Email: m.banzhaf@bham.ac.uk
**Corresponding author. Tel: +44 191 208 3216; Email: w.vollmer@ncl.ac.uk
***Corresponding author. Tel: +31 20 525 3852; Email: t.denblaauwen@uva.nl

FIGURES AND LEGENDS

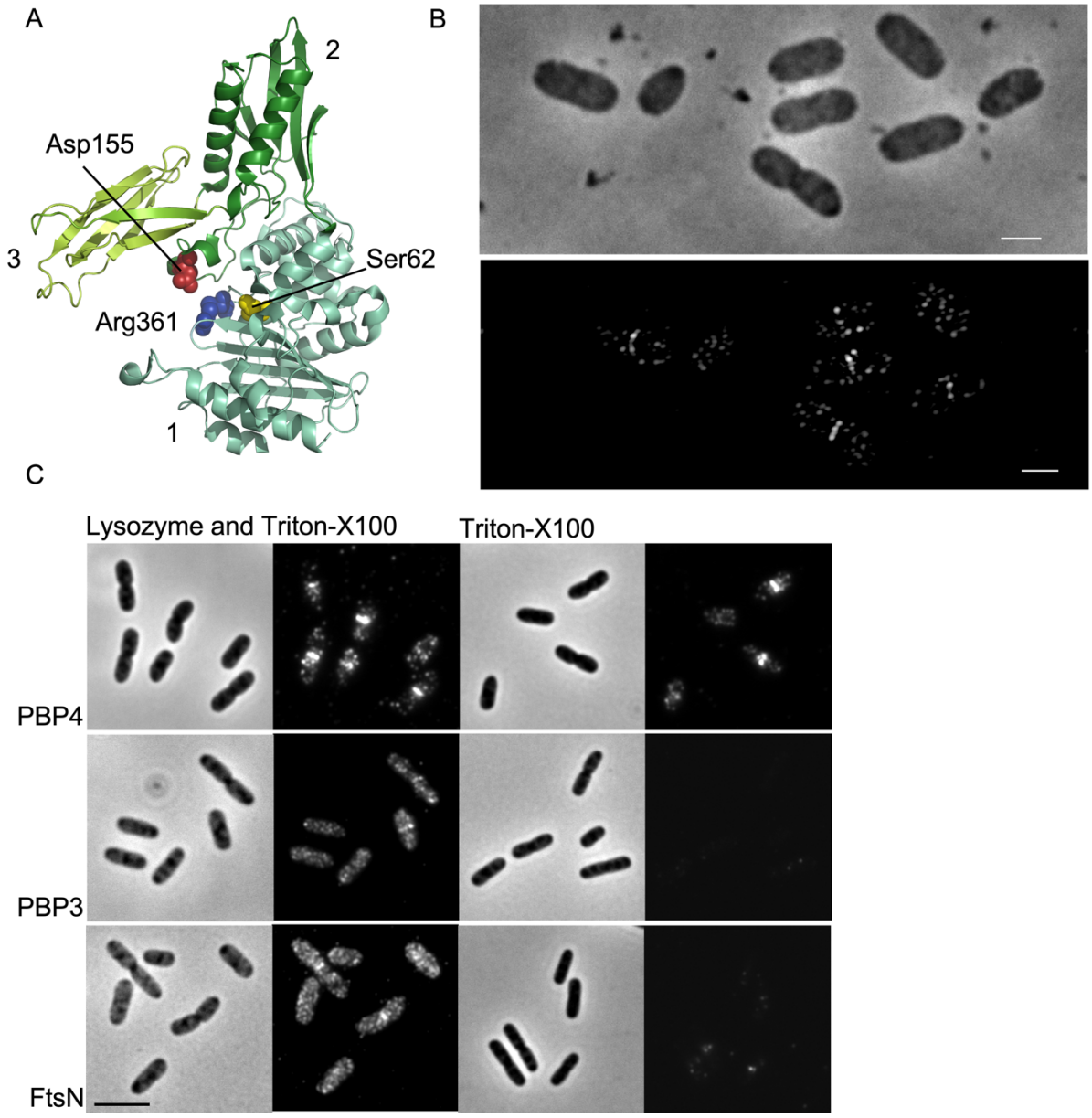

FIG 1 Structure of PBP4 and its localization at midcell and in the lateral wall during fast growth. A. Crystal structure of PBP4 in which the three domains (numbers 1-3) and some of the residues that are essential for its endopeptidase activity are indicated. B. MC4100 cells were grown exponentially in TY medium at 37°C to an OD600 of 0.3 and fixed and immunolabeled with BW25113Δ*dacB* pre-adsorpted anti-PBP4. Upper panel phase contrast image corresponding to the SIM fluorescence image in the lower panel. Scale bar equals 2 µm C. BW25113 wild-type cells were grown in TY at 37°C and harvested in the exponential phase

42 at an OD600 of 0.3 and fixed. Samples were divided into three aliquots and cells were
43 immunolabeled with antibodies against PBP3, FtsN and PBP4. The first aliquot was
44 immunolabeled without any treatment, the second after permeabilizing the cells with
45 TritonX-100 (right: phase contrast and fluorescence images) and the third after
46 permeabilizing cells with Triton-X100 and lysozyme (left: phase contrast and fluorescence
47 images). The scale bar equals 5 µm. PBP4, but not PBP3 or FtsN, is accessible without
48 degrading the peptidoglycan layer.

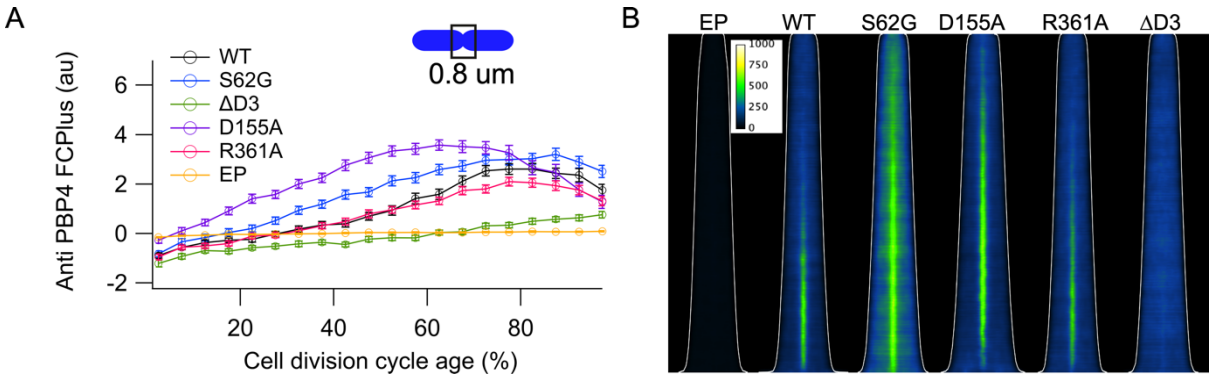

49

50 **FIG 2 Activity of PBP4 is not required for localization.** Cells were grown in minimal glucose
51 medium to steady state at 28°C, fixed and immunolabeled with antibodies against PBP4. (A)
52 The extra fluorescence at midcell (FCPlus) in the Δ*dacB* strain transformed with the empty
53 plasmid (EP, yellow), or plasmids expressing wild-type PBP4 (black), PBP4S63G (blue),
54 PBP4D155A, (purple) PBP4R361A (red), PBP4ΔD3 (green) was determined and plotted as
55 function of the cell division cycle age as in bins of 5% age classes with the error bar indicating
56 the 95% confidence interval. (B) Demographs of the localization fluorescence pattern of the
57 PBP4 variants shown in (A) with the cells sorted according to their cell length. The white line
58 indicates the length of the cells. Intensity scaling is identical for all maps. Number of cells
59 analyzed for each immunolabeling was at least 2000 cells.

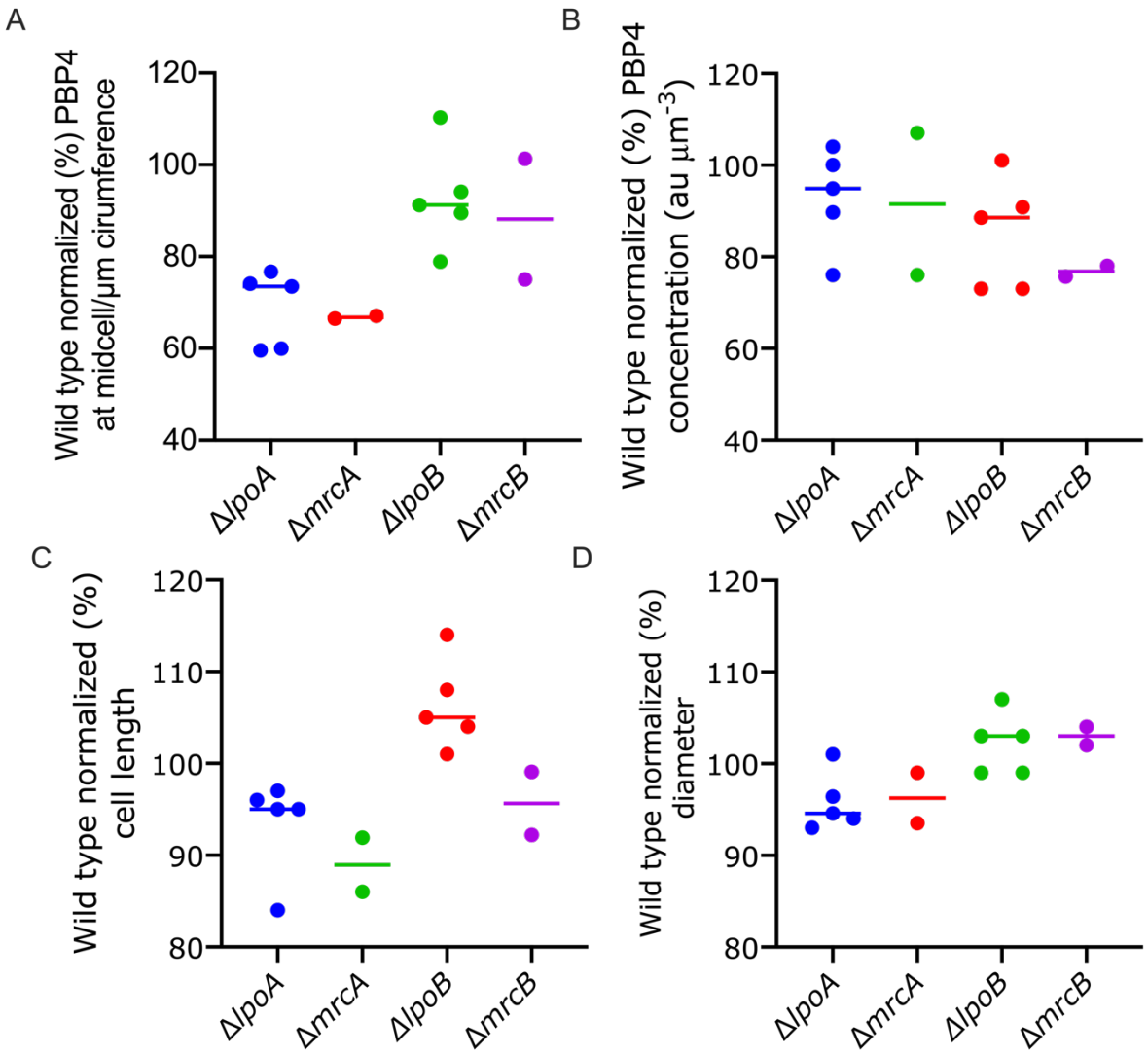

FIG 3 PBP1A and LpoA contribute to PBP4 midcell localization. Cells were grown exponentially to an OD of 0.3 in TY at 37°C, then fixed and immunolabeled with antibodies against PBP4. Because fluorescence imaging by microscopes is usually not directly comparable between different experiments, all results in each experiment were normalized to the parental strain BW25113. (A) PBP4 fluorescence at midcell per µm circumference of the cell. (B) Concentration of PBP4 in the cells. (C) length of the cells. (D) Diameter of the cells. Δ*lpoA* (n=5), Δ*lpoB* (n=5), Δ*mrcA* (PBP1A, n=2), Δ*mrcB* (PBP1B, n=2). Each point is the average of 1000-2000 cells. Based on the one way Anova the difference in midcell localization is

69 significant (P=0.009) while the difference in concentration of PBP4 is not significant

70 (P=0.0484).

71

72 A

73

	K_D of interactions (nM)	
Ligand	PBP4	PBP4ΔD3
LpoA	315 ± 38	153 ± 31
$LpoA^C$	226 ± 15	315 ± 21
$LpoA^N$	954 ± 52	17 ± 4
NlpI	177 ± 49	n.d.[1]
PBP1A	67 ± 9	240 ± 50

[1] no interaction detected.

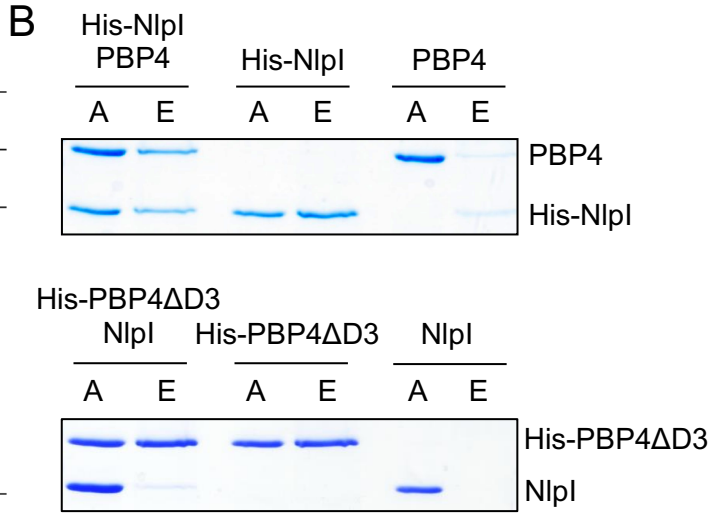

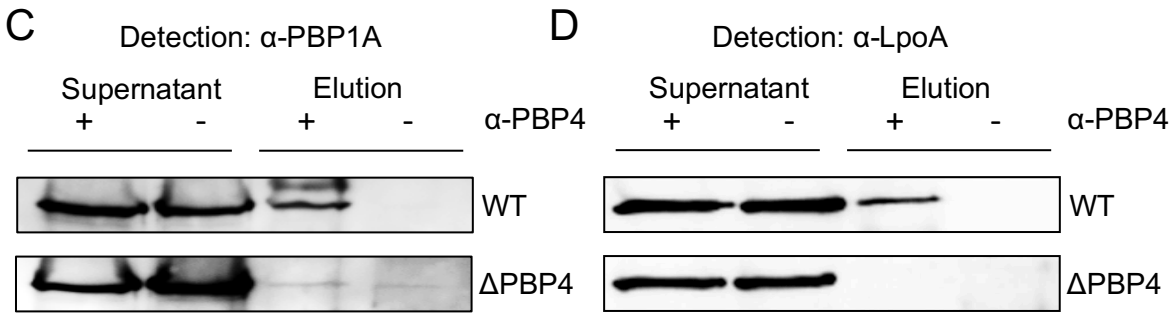

84 **FIG 4 PBP4 interacts with PBP1A, LpoA and NlpI.** (A) Summary of apparent K_D values of the

85 interactions of PBP4 or a version lacking domain 3 (PBP4ΔD3) with LpoA, the C-terminal

86 domain of LpoA ($LpoA^C$), the N-terminal domain of LpoA ($LpoA^N$), NlpI and PBP1A determined

87 by microscale thermophoresis (MST). Corresponding binding curves are shown in Suppl.

88 Figure S7. (B) Pulldown experiment showing that domain 3 of PBP4 is required for interaction

89 with NlpI. Oligo-histidine tagged NlpI (His-NlpI) pulled down PBP4 to Ni-NTA beads. His-tagged

90 PBP3ΔD3 did not pull down untagged NlpI. A, applied sample; E, eluted sample. (C) *In vivo*

91 cross-linking/co-immunoprecipitation showing interaction between PBP1A and PBP4.

92 Growing cells of BW25113 (wt) or BW25113Δ*dacB* (ΔPBP4) were chemically cross-linked with

93 DTSSP and cell extract was immunoprecipitated with purified anti-PBP4 antibody. Control
94 samples did not receive anti-PBP4 antibody. The cross-linker was cleaved by reducing agent
95 and proteins were separated by SDS-PAGE and transferred to a membrane, followed by
96 detection of PBP1A with specific antibodies. PBP1A was detected in the elution of the sample
97 from wild-type and not from ΔPBP4. (D) *In vivo* cross-linking/co-immunoprecipitation (as in
98 panel C) showing that PBP4 and be cross-linked with LpoA in cells.
99

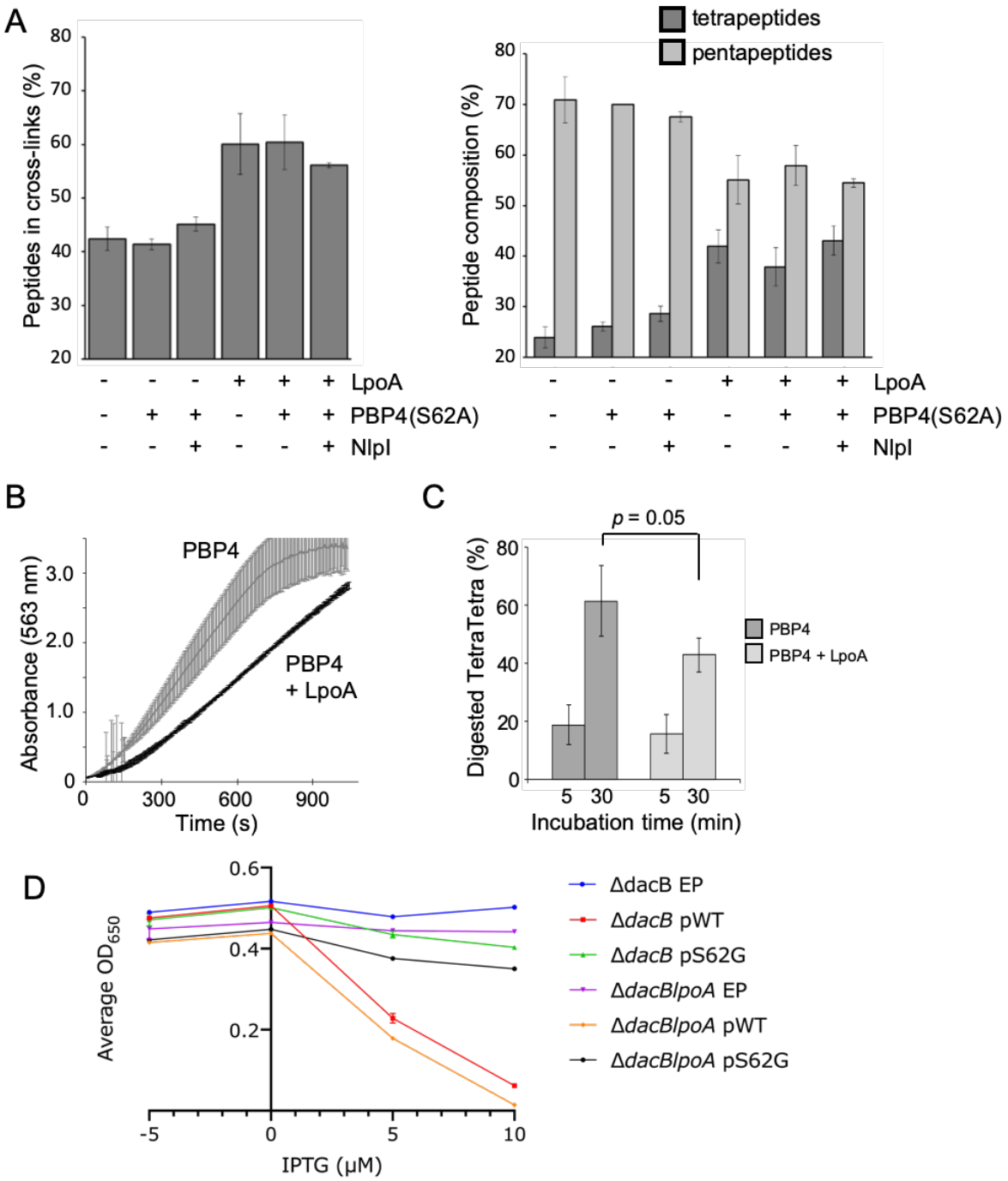

FIG 5 PBP4 or NlpI do not affect the activity of PBP1A whereas LpoA reduces the activity of PBP4. (A) Summary of the results from an *in vitro* PG synthesis assay with PBP1A (in the presence or absence of LpoA) and radio-labelled lipid II substrate. The presence of NlpI, catalytically inactive PBP4(S62A) or both together, does not affect the cross-linkage of the PG product of a PBP1A or PBP1A/LpoA reaction (left side), and NlpI, PBP4(S62A) or both together,

106 don't induce enhanced carboxypeptidase activity of PBP1A, which would be seen as a higher
107 content of tetrapeptides (right side). Values are mean ± variation of two independent repeats.
108 Example chromatograms are shown in Figure S8. (B) The presence of LpoA modestly reduces
109 the activity of PBP4 in a DD-carboxypeptidase assay using the substrate *N*-acetyl-L-Lys-D-Ala-
110 D-Ala. (C) LpoA also reduces slightly the activity of PBP4 against PG sacculi from BW25113, as
111 seen by the reduced digestion of TetraTetra upon a 30 min incubation period.
112 (D The Δ*dacB* and Δ*dacB*Δ*lpoA* mutant strains are equally sensitive to overexpression of PBP4.
113 The average growth over time as measured by OD650 nm is plotted against the added IPTG
114 concentration. The culture grown in TY with glucose to suppress the expression is represented
115 by -5 on the X-axe. All other data points are from cell grown in TY without glucose (n=4).
116

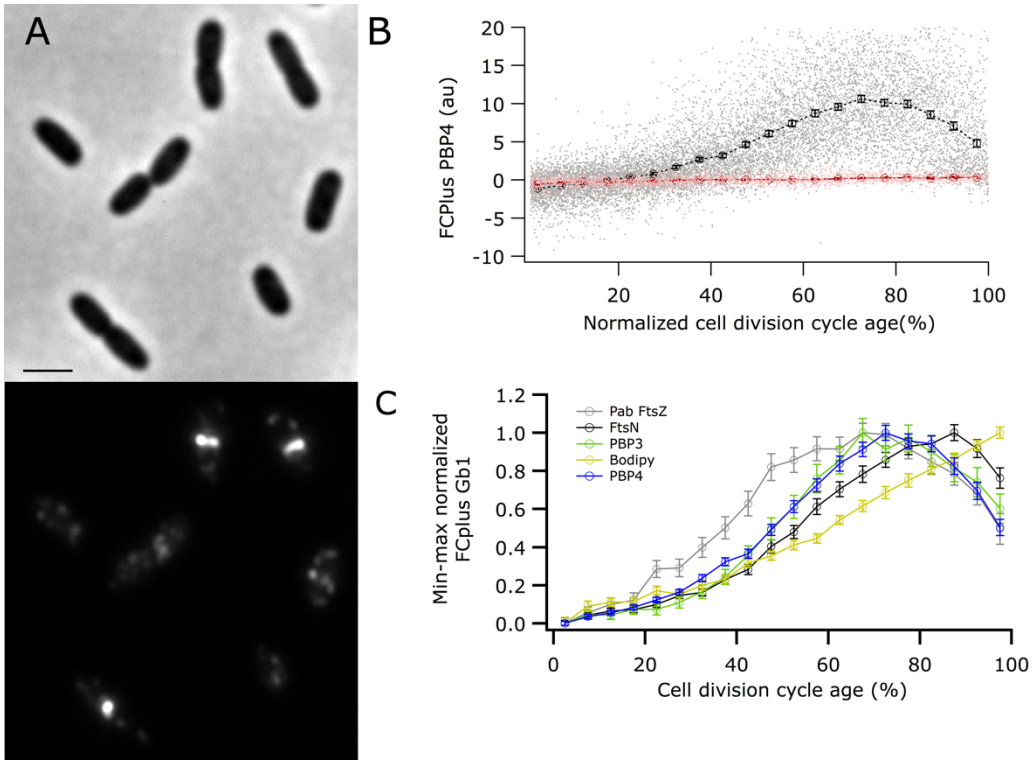

117

118 **FIG 6 Cell division cycle timing of the localization of PBP4. (**A) MC4100 cells were grown to
119 steady state in minimal glucose medium at 28°C and immunolabeled with antibodies specific
120 for PBP4. Phase contrast (top) and fluorescence is shown (bottom). Scale bar equals 2 µm. (B)

121 The extra fluorescence at midcell compared to the rest of the cell (FCPlus) is plotted as
122 function of the normalized cell division cycle age. The dots (grey for MC4100 and light pink
123 for the BW25113 Δ*dacB strain*) are the values measured for the individual cells and the
124 markers with bars (black for the wild-type MC4100, red for the BW25113 Δ*dacB*) are 5% age
125 bins with 95% confidence. (C) Comparison of the timing of the localization at midcell of FtsZ
126 (grey), PBP4 (blue), PBP3 (green) and FtsN (black) and the general membrane stain bodipy-12
127 (yellow) during the cell division cycle age. The FCPlus values are min-max normalized to
128 enable timescale comparison, despite differences in molecule number and antibody affinities.
129

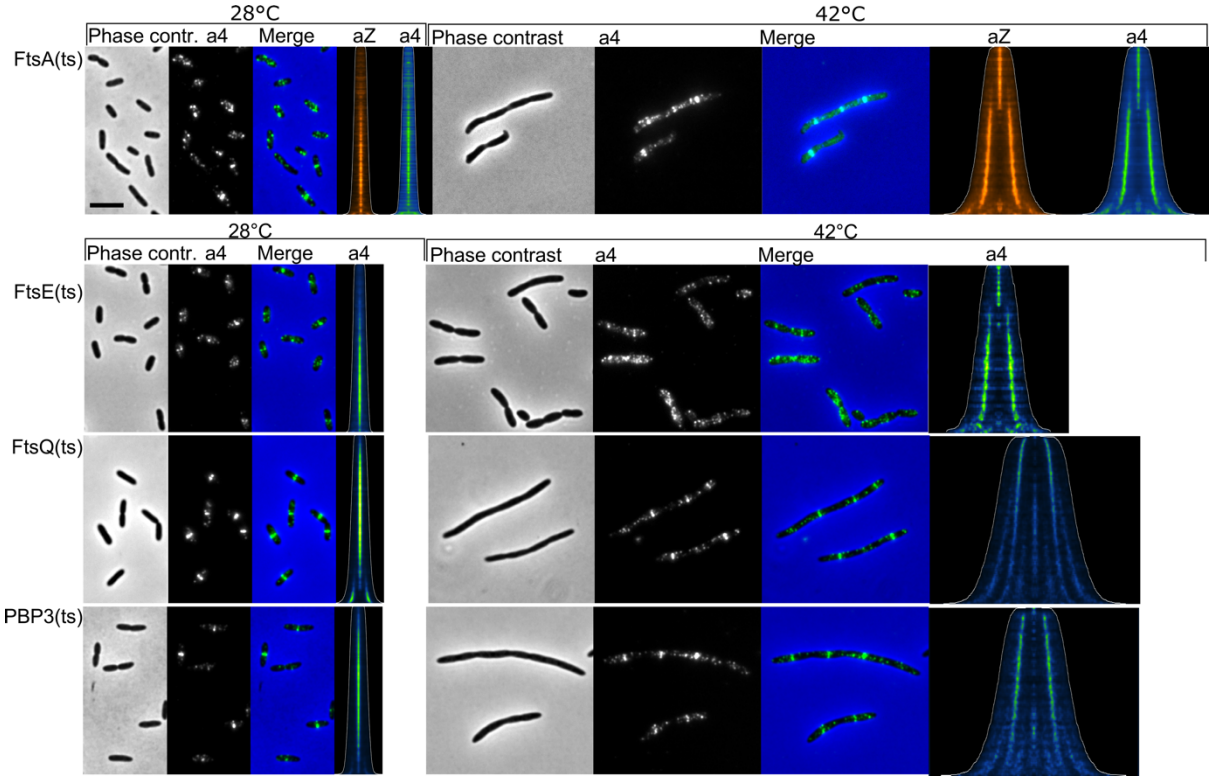

130

131 **FIG 7 PBP4 localization is dependent on the presence of the proto-ring.** Isogenic strains
132 producing different temperature sensitive (ts) versions of cell division proteins where grown
133 to steady state in Gb1 medium at 28°C and split in two parts. These were 1:4 diluted in
134 prewarned medium and grown for two mass doublings (MD) at either 28°C or 42°C. The cells

135 were fixed, labeled with antibodies specific for PBP4 (a4) and, in the case of FtsA (ts), with
136 antibodies against FtsZ (aZ). From left to right: the phase contrast, corresponding
137 fluorescence image of the PBP4 labeling and the merged images at the permissive
138 temperature, demograph of PBP4 fluorescence localization where cells are sorted according
139 to their cell length (contours in white). This is followed by the same series from the non-
140 permissive temperature samples. The number of cells analyzed were 3641 and 1642 for
141 LMC511 FtsA (ts), 2809 and 1576 for LMC515 FtsE(ts), 3833 and 1203 for LMC531 FtsQ (ts)
142 and 3876 and 926 for LMC510 PBP3(ts), for the cells grown at 28°C and 42°C, respectively.
143 The scale bar equals 5 µm.

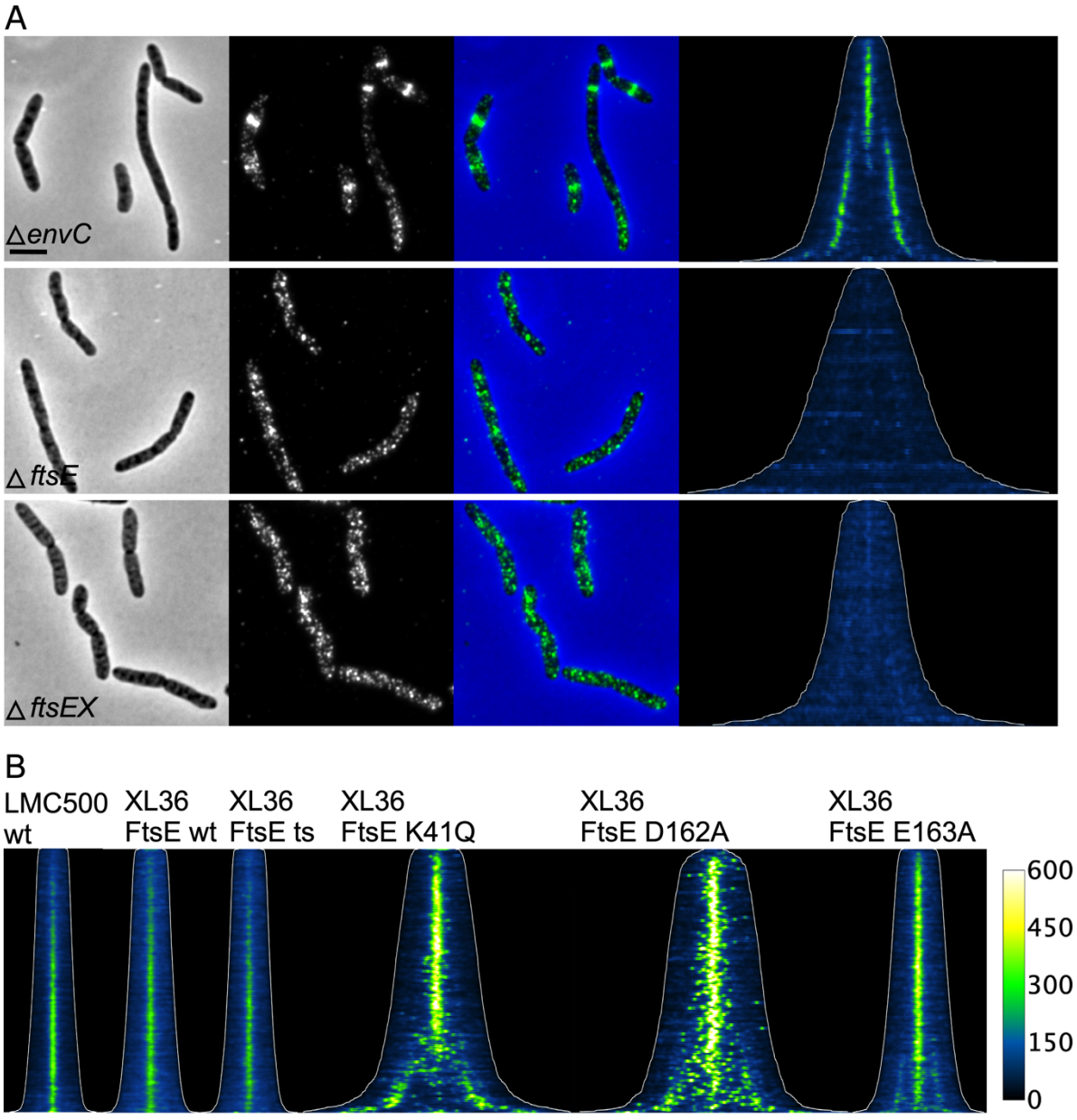

FIG 8 PBP4 is recruited by the septal cleavage complex FtsEX. (A) Cells of BW25113 expressing the proteins indicated were grown in LB at 37°C to OD_{600} = 0.3, fixed and labeled with specific antibodies against PBP4. From left to right, the phase contrast, corresponding fluorescence image of the PBP4 labeling, and the merged former two images, map of fluorescence with the cell lengths outlined (with the same contrast and brightness for all maps) of PBP4 localization where cells are sorted according to their cell length are shown. The number of cells analyzed were 687 for Δ*envC*, 434 for Δ*ftsE*, and 346 for Δ*ftsEX*. The scale bar equals 5 μm. (B) Cells of LMC500 or XL36 (LMC500Δ*ftsE*::p*Trc99A*down *fts*X) expressing wild-

153 type or active site versions of FtsE were immunolabeled with anti-PBP4 antibodies. Cells were

154 grown in TY at 30°C and FtsE expression from plasmid was induced for 2 mass doubling with

155 30 μM IPTG, and cell were fixed and harvested at an OD_{600} of 0.3. The maps of PBP4

156 fluorescence with the cell lengths outlined is shown for the indicated strains. Number of cells

157 analyzed: LMC500 (2462), (wt) (2588), (ts) (2540), K41Q (728), D162A (554), and E163E (1052).

158

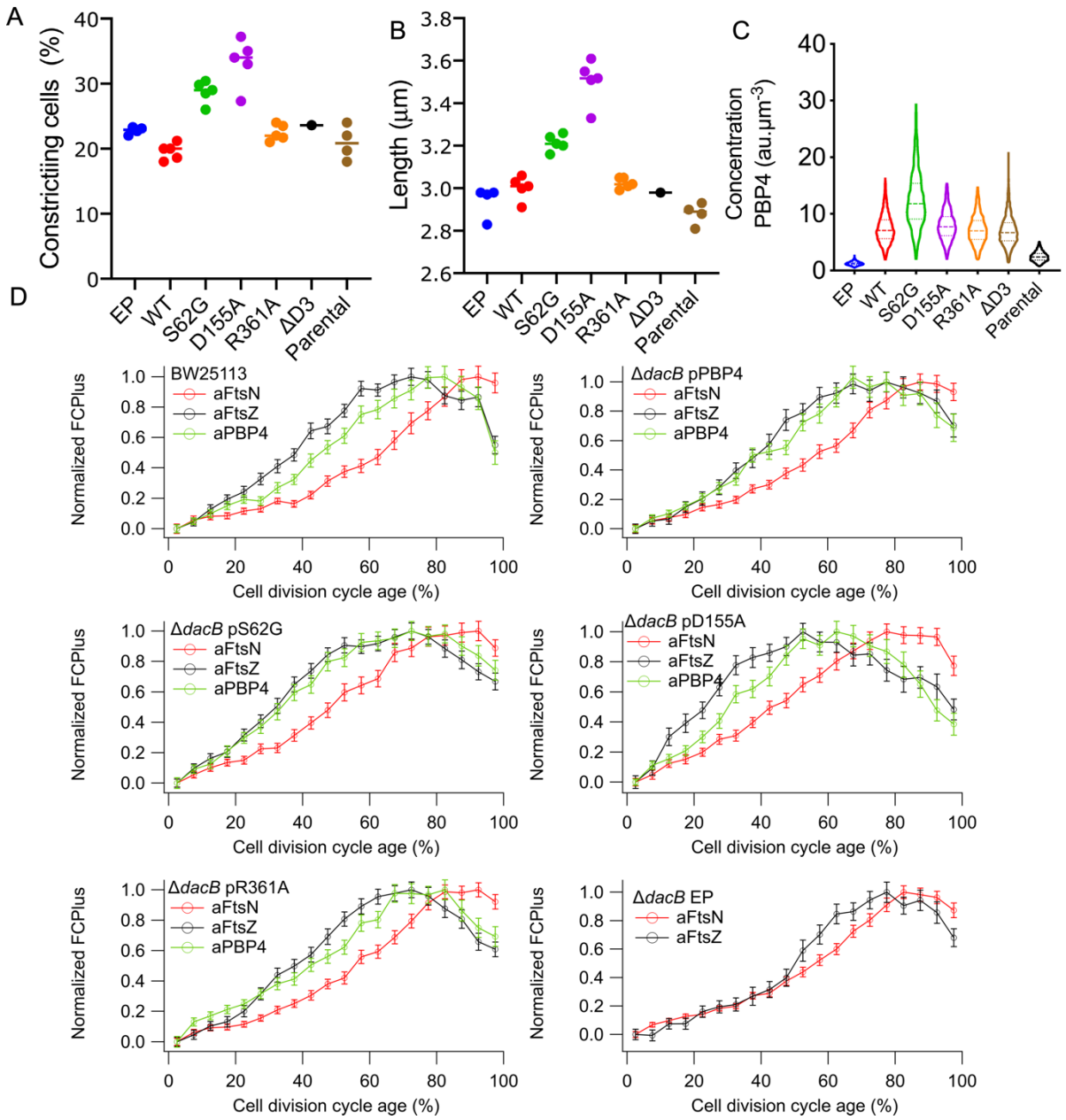

159

160 **FIG 9 Localization of PBP4 depends on the presence of domain 3 but not on activity.** Cells
161 were grown in minimal glucose medium to steady state at 28°C, fixed and immunolabeled
162 with the indicated antibodies. (A and B) Graphs with the percentage of constricting cells and
163 the average cell length in μm for the various mutants expressed from plasmid in the Δ*dacB*
164 strain and also of the parental strain BW24113 (n = 4). (C) The concentration of PBP4 in
165 fluorescent units per μm^3 in these cells for a representative experiment (out of the four
166 repeats).
167 (D) Normalized FCplus of FtsN, FtsZ, and PBP4 plotted against normalized cell division cycle
168 age for the parental strain BW25113, the Δ*dacB* strain carrying plasmids for the expression of
169 PBP4WT, PBP4S63G, PBP4D155A, PBP4R361A or no protein (EP) showing that despite having
170 a relative normal length and constriction percentage, FtsZ and FtsN localize rather late at
171 midcell in the Δ*dacB* strain. Plasmids were not induced.
172

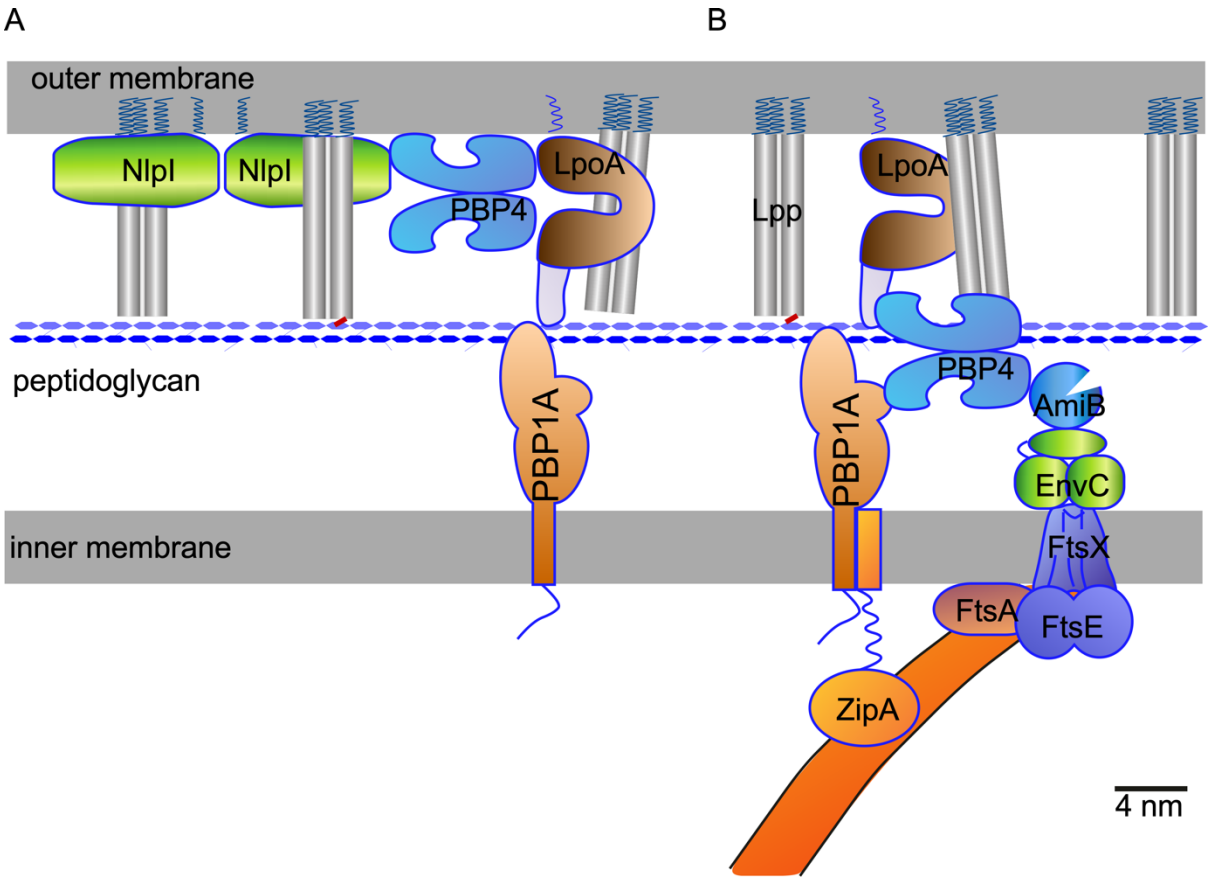

173

174

175 **FIG 10 Model of the organization of PBP4 in the periplasm of *E. coli*.** In a minimal medium
176 grown cell of average size of 3 by 0.86 µm 230000 Lpp trimeric proteins are present of which
177 1/3 is bound to PG. (A) During elongation PBP4 (or a fraction of the PBP4 molecules) is kept
178 away from its substrate through its interaction with NlpI and possibly LpoA. (B) PBP1A and
179 LpoA associate with ZipA and the Z-ring to assist in preseptal PG synthesis. Because of their
180 presence, the absence of NlpI and the newly synthesized PG, PBP4 is attracted by PBP1A and
181 LpoA. More PBP4 is accumulating at midcell and becoming clearly visible by immunolabeling
182 upon maturation of the divisome and synthesis of septal PG. All proteins apart from the FtsZ
183 polymer have been drawn according to their crystal structure shape and hydrated crystal
184 structure sizes (scale bar equals 4 nm). The membranes are assumed to be 2 nm and the
185 distance between the outer and the inner membrane 21 nm.